Analysis of atmospheric CH_4 in Canadian Arctic and estimation of the regional CH_4 fluxes

Misa Ishizawa[1], Douglas Chan[1], Doug Worthy[1], Elton Chan[1], Felix Vogel[1] and Shamil Maksyutov[2]

5 [1]Environment and Climate Change Canada, Toronto, M3H 5T4, Canada
[2]National Institute for Environmental Studies, Tsukuba, 305-8506, Japan

Correspondence to: Misa Ishizawa (misa.ishizawa@canada.ca)

Abstract. The Canadian Arctic (>60˚N, 60˚W─141˚W) may undergo drastic changes if the Arctic warming trend continues. For methane (CH_4), Arctic reservoirs are large and widespread, and the climate feedbacks from such
10 changes may be potentially substantial. Current bottom-up and top-down estimates of the regional CH_4 flux range widely. This study analyses the recent observations of atmospheric CH_4 from five arctic monitoring sites and presents estimates of the regional CH_4 fluxes for 2012─2015. The observational data reveal sizeable synoptic summertime enhancements in the atmospheric CH_4 that are distinguishable from background variations, which indicate strong regional fluxes (primarily wetland and biomass burning CH_4 emissions) around Behchoko and Inuvik in the western
15 Canadian Arctic. Three regional Bayesian inversion modelling systems with two Lagrangian Particle Dispersion Models and three meteorological datasets are applied to estimate fluxes for the Canadian Arctic and show relatively robust results in amplitude and temporal variations across different transport models, prior fluxes and sub-region masking. The estimated mean total CH_4 flux for the entire Canadian Arctic is 1.8 ± 0.6 TgCH4 yr^{-1}. The flux estimate is partitioned into biomass burning of0.3 ± 0.1 TgCH4 yr^{-1}, and the remaining natural (wetland) flux of 1.5 ± 0.5
20 TgCH4 yr^{-1}. The summer natural CH_4 flux estimates clearly show inter-annual variability that is positively correlated with surface temperature anomalies. This indicates that the hot summer weather conditions stimulate wetland CH_4 emissions. More data and analysis are required to statistically characterise the dependence of regional CH_4 fluxes on the climate in the Arctic. These Arctic measurement sites will aid in quantifying the inter-annual variations and long-term trends in CH_4 emissions in the Canadian Arctic.

25 **1 Introduction**

Atmospheric methane (CH_4) is one of the principal greenhouse gases with a global warming potential (GWP), 34 times stronger than carbon dioxide (CO_2) over a 100 year time period, and 96 times stronger over a 20 year time period (Gasser et al., 2017). Atmospheric level of CH_4 has doubled since the pre-industrial era, from about 722 ppb to 1803 ppb in 2011 (Ciais et al., 2013). Natural wetland CH_4 emission in Arctic regions is of much interest to the scientific
30 community because the CH_4 emissions can potentially increase in a warming climate (AMAP, 2015). The Arctic is underlain with continuous permafrost containing large quantities of soil carbon, ~1700 PgC, (Tarnocai et al., 2009). Under warming scenarios, this stored carbon may be highly vulnerable to conversion to CH_4 and CO_2, which can be emitted to the atmosphere. However, there is only low confidence in the exact magnitude of CO_2 and CH_4 emissions

caused by the permafrost thawing and whether carbon will decompose aerobically to release CO_2 or anaerobically to release CH_4 (e.g. McGuire et al., 2009; Schuur et al., 2015; Thornton et al., 2016).

Natural CH_4 flux estimates are highly uncertain in northern high latitudes. There have been many studies on CH_4 emission using both bottom-up and top-down methods. A thorough review of these studies can be found in Saunois et al. (2016). In general, bottom-up flux estimates for the northern high latitudes from biogeochemical CH_4 models have large variations with the mean estimates being much higher than top-down estimates from inverse modelling (Saunois et al., 2016). For the Boreal North America region including Alaska and the Hudson Bay Lowlands (HBL, the second largest boreal wetland in the world), the bottom-up mean estimate is ~32 $TgCH_4$ yr^{-1}, with a wide range from 15 to 60 $TgCH_4$ yr^{-1}. On the other hand, the top-down mean estimate is ~12 $TgCH_4$ yr^{-1} with a narrower range from ~7 to 21 $TgCH_4$ yr^{-1}.

Bottom-up estimates from wetland methane models in WETCHIMP show large discrepancies in the spatial distribution of wetlands CH_4 source, as well as its magnitude (Melton et al., 2013). In the higher latitudes, the limited ground-based information has hindered the mapping of wetland area. Recently, remote sensing provided more information, but the high-latitude wetland extent still contains large uncertainties (Olefeldt et al., 2016; Thornton et al., 2016). In addition to uncertainty in wetland extent, other factors affecting high-latitude wetland emissions in different models still remain. In a recent inter-comparison of CH_4 wetland models (Poulter et al., 2017) , all models used the same wetland extent, Surface Water Microwave Product Series (SWAMPS) (Schroeder et al., 2015) with Global Lakes and Wetland Database (GLWD) (Lehner and Döll, 2004) and the same meteorological data (CRU-NCEP v4.0 reconstructed climate data) to drive their models. The models showed a large range in estimated CH_4 emission for North American Boreal/Arctic region, compared to other regions in the world. This large range of the CH_4 emissions for North American Boreal/Arctic region clearly shows the uncertainty in our current understanding of the physical and biogeochemical processes that contribute to wetland CH_4 emissions.

Top-down atmospheric inverse models have been developed to infer fluxes with observed atmospheric CH_4 mixing ratios as constraints. Global CH_4 inversion studies estimate global distribution of emissions and sinks from observational sites from around the world (e.g. Bousquet et al., 2011; Bergamaschi et al., 2013; Bruhwiler et al., 2014), but with very limited observational information in northern high latitudes for these studies. Recently ground-based observational coverage in northern high latitudes improved with the expansion of towers and aircraft atmospheric observing platforms in Arctic regions (e. g. Karion et al., 2016; Sasakawa et al., 2010; Chang et at., 2014).   These observations have been used for CH_4 flux estimation in specific regions. For North America, previous atmospheric CH_4 studies were mainly focused on Alaska (e.g. Miller et al., 2016; Hartery et al. 2018). Thompson et al., (2017) conducted CH_4 flux estimates for the entire region north of 50°N, combining recent high-latitude surface observations. Estimated CH_4 emissions for the Canadian Arctic (representing the land region of Canada north of 60°N) show discrepancies among the inverse studies; the mean total CH_4 emission (2006-2010) is ~1.8 $TgCH_4$ by TM5-4DVAR (Bergamaschi et al., 2013), 0.5 $TgCH_4$ by CarbonTracker-CH_4 (Bruhwiler et al., 2014), and 2.1 $TgCH_4$ by FLEXINVERT (Thompson et al., 2017). Differences including model transports, prior fluxes and observational datasets could affect the inversion results. The previous CH_4 inversion studies used only observations from Alert in

the Canadian Arctic, the most northern observational site in the world. Several new sites in the Canadian Arctic (described in the next paragraph) might be helpful in constraining flux estimation.

Canada has a vast Arctic/sub-Arctic region (~39% of Canada's total land) with wetlands and permafrost. It is important to study the methane cycle and monitor the effects of climate change in this sensitive region as these
5   effects could impactatmospheric CH_4 levels at national, continental and hemispheric scales. Environment and Climate Change Canada (ECCC) has recently added five greenhouse gas (GHG) measurement sites in northern Canada to monitor the time evolution of Arctic GHGs in view of better constraining flux estimates in the region. In October 2010, ECCC started continuous GHG measurements at Behchoko (BCK, 115.9˚W, 62.8˚N), the first ground-based site of continuous measurements in the Canadian Arctic, other than Alert (ALT, 82.5˚N, 62.5˚W) where continuous
10   measurements was implemented in 1988. Following BCK, additional continuous measurement programs were implemented at Churchill (CHL, 58.7N, 93.8W) in 2011, Inuvik (INU, 68.3˚N, 133.5˚W), Cambridge Bay (CBY, 69.1˚N, 105.1˚W) in 2012, and Baker Lake (BLK, 64.3˚N, 96.0˚W) in 2017.

We present the first study to analyse the atmospheric CH_4 mixing ratios from the above new ECCC observational sites located in the Canadian Arctic region. In this study, we address three key questions: (1) what
15   information can these new measurements provide in regards to local and regional sources? (2) what are the estimated CH_4 fluxes in the Canadian Arctic using inverse modelling with these new measurements? (3) are there any relationships between the Canadian Arctic CH_4 fluxes and climate/environmental variations? This paper is structured as follows: In Sect. 2, the description of the measurement sites as well as the observational data analyses from daily to inter-annual time scales are given. Section 3 describes the inversion model framework. Section 4 presents flux
20   estimates along with flux uncertainties and potential correlations with climate anomalies.

2 Measurements

ECCC operates six measurement sites in the Canadian Arctic region to monitor the GHG mixing ratios. Alert (ALT) is the most northern GHG monitoring site on the globe. Weekly flask samples for CO_2 measurements began in 1975. Continuous CH_4 measurement started in 1988. The other five Arctic/sub-Arctic sites, Behchoko (BCK), Churchill
25   (CHL), Inuvik (INU), Cambridge Bay (CBY), and Baker Lake (BLK) gradually became operational starting in 2007. BLK is the most recent site in the Canadian Arctic with continuous measurement started in July 2017, which augmented the flask air sampling measurement program (started in 2014). At the four other sites, continuous measurement systems were initiated during the period of 2010–2012. The observations from these four sites were used for the inversion in this study. Further detailed site information of all six measurement sites are in Table 1, A
30   map showing their locations is in Fig. 1. Currently, all ECCC continuous measurements are conducted using in-situ cavity ring-down spectrometer (CRDS, Picarro G1301, G2301 or G2401), and discrete flask air samples are measured using a gas chromatograph equipped with flame ionisation detectors (GC-FID, Agilent 6890). Both measurements are traceable to World Meteorological Organization (WMO) X2004 scale (Dlugokencky et al., 2005). In the following sections, we describe the sites briefly and characterise the observed variations of the CH_4 mixing ratios at the sites.

2.1 Site Descriptions

Alert (ALT, 82.5^{0}N, 62.5^{0}W) being located thousands of kilometres from major GHG source regions is often referred to as an Arctic background site. The Alert observatory is located ~6 km away from the main military base camp. The lack of local source surrounding the site results in no significant diurnal variation in observed atmospheric CH_4 mixing

5   ratios throughout the year. In winter, under weak vertical mixing, well-defined synoptic variations are observed due to inter-continental scale transport along with mainly anthropogenic CH_4 originating from the Eurasia continent (Worthy et al., 2009). The measurements at Alert typically represent large-scale background conditions and thus ideal for providing information on the long-term trend and seasonal cycle for the Arctic (Worthy et al., 2009).

10   **Behchoko (BCK, 62.8°N, 115.9°W)** is located on the northwest tip of Great Slave Lake. The continuous measurement program started in October 2012. Flask sampling is not conducted at this site. The air sampling intake is installed at the top of a 60 m communication tower. The observational equipment is placed in a small isolated room in a local backup power generation station that is rarely turned on. BCK is located 10 km away from the town of Behchoko that is a community ~80 km northwest of Yellowknife, the capital of the Northwest Territories. Mixed forests, lakes and

15   ponds surround the BCK site.

Inuvik (INU, 68.3°N, 133.5°W) is located ~120 km south of the coast of the Arctic Ocean. The continuous measurement program started in February 2012. Flask sampling began in May 2012. The measurement system is located in the ECCC upper air weather station building, 5 km southeast of the town of Inuvik. INU is ecologically

20   surrounded by Arctic tundra and geologically located in the east channel of the Mackenzie Delta, where a number of water streams and ponds are formed, and vast hydrocarbon deposits are found. Although there are proposed developments of natural gas and pipeline project, most have been on hold.

Cambridge Bay (CBY, 69.1°N, 105.1°W) is on the southeast coast of Victoria Island. CBY is located ~1 km north

25   of the town of Cambridge Bay, the largest port of the Arctic Ocean's Northwest Passage. Both continuous and flask sampling measurements started in December 2012. The measurement system is located in the ECCC upper air weather station building.

Baker Lake (BKL, 64.3°N, 96.0°W) is located on the shore of Baker Lake, ~320 km inland of Hudson Bay. Weekly

30   flask air sampling started in June 2014, and the continuous measurement program in July 2017. The air sampling system is located in the ECCC upper air weather station.   BCK is in an Arctic tundra region, surrounded by small lakes.

Churchill (CHL, 58.7°N, 93.8°W) is located on the west coast of Hudson Bay. The GHG monitoring program began

35   with flask air sampling in 2007. The continuous observational program started in October 2011. The sampling equipment is placed in the Churchill Northern Studies Research Facility, ~23 km east of the town of Churchill. CHL

is situated in an area with Arctic tundra to the north and on the northern perimeter of the Hudson Bay Lowlands, the largest contiguous boreal wetland region in North America.

2.2 Temporal Variations

Figure 2 shows a time-series of CH_4 mixing ratios; hourly means, afternoon means (using hourly data from
5   12:00─16:00 local time), and values from flask sampling for each site. The fitted curve and long-term trend were generated using the merged data containing both continuous afternoon means and flask data. The curve-fitting method has two harmonics of one-year and half-year cycles along with two low and high pass digital filters with cut-off periods of 4 months and 24 months respectively (Nakazawa et al., 1997).

       Overall, the features of the continuous and flask measurements show similar long-term trend and seasonal
10   cycles. The continuous measurements reveal short timescale variations that are less visible in the flask data records. The diurnal and synoptic variations of atmospheric CH_4 provide information on local and regional scale interactions between the atmosphere and the source fluxes (Chan et al., 2004).

       All the sites show similar upward trends of atmospheric CH_4. The growth rates observed at the Canadian Arctic sites are comparable to the global mean growth rates based on the global network of National Oceanic and
15   Atmospheric Administration (NOAA) air sampling (www.esrl.noaa.gov/gmd/ccgg/trends_ch4/, Fig. S1). In 2014, the growth rates jumped at all the sites except BCK. In the following year 2015, the growth rates dropped but were still higher than the growth rates prior to 2014. The rapid enhancement in growth rates at the Canadian Arctic sites is consistent with the globally averaged atmospheric CH_4. The 2014 growth rate at BCK was also enhanced, but the enhancement was not as high as those at the other Arctic sites were. This moderate growth rate for BCK might be an
20   artefact in its long-term component partially due to a two month period of missing data (mid-November 2014 to mid-January 2015).

2.2.1 Seasonal and inter-annual variations

Since the long-term trends reflect the global-scale source/sink changes, the long-term component at ALT is subtracted from all the sites in order to isolate the regional scale signals in the observed atmospheric CH_4 data records (Fig. 3).
25   The mean seasonal cycles show a maximum in winter and a minimum in summer. All sites show a similar pattern with a maximum in January/February, while the differences are more noticeable in summer. The summer minimum that is typically representative of the large-scale Arctic background can be seen from July to August at ALT. The summer minima at the other Arctic sites are generally enhanced (with higher CH_4 mixing ratios) relative to ALT, and very considerably amongst the sites and from year to year. These enhancements and inter-annual variability are due
30   to the superposition of the enhanced atmospheric CH_4 sink and increased wetland emissions during warm seasons. Minima are seen in June at BCK, INU and CHL, followed by BKL and CBY with ~1 to 1.5 month lags.   Another interesting feature seen at INU, BCK and CHL is a secondary maximum in summer (a summer bump), also indicative of the influence of local/regional wetland and biomass burning emissions. As seen in Figure 3, these secondary maxima/summer bumps vary in timing and amplitude from year to year. The bumps were observed at BCK, INU and
35   CHL in 2012, which were in phase with each other, but not at any site in 2013. In 2014, a more substantial summer

bump was observed at BCK than 2012 (2014 has strong biomass burning contributions) while the summer bump at CHL was similar to the one in 2012. The cause(s) for the "summer bumps" at BCK, CHL and INU, might vary year-to-year, such as local/regional (wetland and forest fires) emission change due to climate anomaly. Another possible cause is inter-annually varying atmospheric transport.

5 **2.2.2 Synoptic and diurnal variability**

All measurements of atmospheric CH_4 in the Canadian Arctic show synoptic and daily variations with seasonally changing amplitudes. One quantitative measure of synoptic variability in the observed CH_4 mixing ratios is the monthly Standard Deviation (SD) of the residual of observed time series relative to their fitted curves. Figure 4 shows the mean seasonality in SD of all 24 hourly data (SD_24) in CH_4 mixing ratios at each site except BKL, as well as the
10 mean seasonality of the afternoon hourly data (SD_PM). Although SD_24 and SD_PM appear similar (some are almost identical) except during summer months, the differences between SD_PM and SD_24 provide a measure if the daily variability is reflecting a local scale change in emission or rather a change on the atmospheric transport processes. The nighttime planetary boundary layer (PBL) is usually shallow, while the daytime boundary layer is usually deeper and well mixed. If there are local CH_4 sources, the emission will be mixed into a shallow PBL at night (yielding
15 higher mixing ratio) and diluted through a deeper PBL during the day (yielding lower mixing ratio). The resultant diurnal variations in the CH_4 mixing ratios are evident as larger CH_4 SD_24 compared to SD_PM. In the absence of local sources, SD_24 is comparable to SD_PM.

The most substantial synoptic variations are observed in summer at all sites except ALT (Fig. 4). This indicates that the major regional CH_4 emissions in the continental Canadian Arctic occur in summer. At ALT, the
20 largest synoptic variations are observed in winter. The winter synoptic variations are mainly due to strong long-range transport from other regions which has been demonstrated for ALT (Worthy et al., 2009).

The diurnal variability of atmospheric CH_4 is mainly caused by a local CH_4 emission signal modulated by daily PBL development, or a temporal change of the local source. In summer, the SD_24 values are higher by > 5ppb than the SD_PM except for ALT. The larger SD_24 in summer supports the existence of local CH_4 sources around
25 the sites, likely wetland CH_4 emissions. In contrast, the fact ALT has identical SD_24 and SD_PM all year round confirms that there is no significant local source near the site.

Similar to the three continental sites (BCK, INU, CHL), CBY also shows the maxima of SD_24 and SD_PM in summer, but they remain lower than BCK, INU and CHL, but higher than ALT. This indicates that there is a weaker local source of CH_4 around CBY than around the three continental sites. In the cold season (September to May), the
30 SD_24 and SD_PM at CBY are almost identical to ALT. It is noticeable that the SD_24 and SD_PM at BCK, INU and CHL are still higher than ALT until December. These higher SD_24 and SD_PM values in the first half of the cold season might indicate possible CH_4 emissions from the ground. Zona et al. (2016) suggested that there are on-going CH_4 emissions from the Alaskan Arctic tundra during the "zero curtain" period when the soil temperature is near zero with average air temperature below 0°C until the surface is completely frozen.
35 The SD_24 and SD_PM for winter to spring (January to May) at INU remain higher than the other sites. Also, SD_24 at INU becomes higher than SD_PM from April and remains higher over summer. At the other sites,

the difference between SD_24 and SD_PM are seen mainly in the summer months (June—August). This higher variability in atmospheric CH_4 at INU in winter and spring, when the surrounding wetland ecosystem is inactive, likely indicates strong local CH_4 sources, such as anthropogenic CH_4 emissions from natural gas well/refinery facilities. During winter, such local CH_4 signals are amplified by the seasonally calm condition (the mean seasonal cycles of wind speed are shown in Fig. S2 in the Supplemental Information Section) and by reduced vertical mixing within the shallow PBL due to the shorter period of daylight in the polar region. Figure S3 shows the deviations (from the fitted curve) of observed hourly and afternoon mean CH_4 at INU and BCK along with wind speed. In April and May, the difference of deviations between hourly CH_4 and afternoon mean CH_4 becomes larger again after the relatively quiet period. This may indicate the signals of local (anthropogenic) emission around INU being amplified as the PBL diurnal variation starts developing due to longer daytime periods. Another possible local source for the large spring SD_24 and SD_PM at INU may be the natural CH_4 emissions originating from lakes and ponds during the spring thaw (Jammet et al., 2015). In contrast, SD_24 and SD_PM at BCK become smaller as the wind speed increases, indicating a lack of local CH_4 source around BCK in spring.

Since ALT is representative of the Arctic background state in synoptic variability, the difference of SD_24 or SD_PM between ALT and each of other sites gives a measure of the regional source influence to the site. The sizeable regional source influence signals in summer shown in Figure 4 should be useful in constraining the regional flux estimation modelling in the next sections.

3 Regional inversion model description

To estimate the regional CH_4 fluxes in the Canadian Arctic, we apply a Bayesian inversion approach, based on the backward simulations by Lagrangian Particle Dispersion Models (LPDM). In this study, three different transport models and three prior CH_4 flux distributions were used to help estimate the model uncertainties. The following sections describe the various components of our regional inverse modelling.

3.1 Transport models and meteorological data

LPDMs simulate an ensemble of air-following particles which are released from the measurement sites. The air particles travel backwards in time for 5 days with the wind field. Previous studies (e.g. Cooper et al., 2010; Gloor et al., 2001; Stohl et al., 2009) have shown 5 days are typically sufficient to capture the surface influence to a measurement site from the surrounding region. The backward trajectories are used to calculate the footprints as the integrated residence times the particles spent inside the PBL at a resolution of 1.0°×1.0°. We use three different regional model setups combining two different LPDMs: FLEXPART and STILT, and three different meteorological data from the European Centre for Medium-range Weather Forecasts (ECMWF), Japanese Meteorological Agency (JMA), and Weather Research and Forecasting model (WRF).

LPDMs simulate local contributions for 5 days prior to the measurements at sites. The background condition of atmospheric CH_4 mixing ratios at the endpoints of the particles is provided by a global model, National Institute for Environmental Studies-Transport Model (NIES-TM) with global CH_4 flux fields. Below are the details of model setups in this study.

3.1.1 LPDM: FLEXPART_EI

The first model setup is FLEXible PARTicle dispersion model (FLEXPART) (Stohl et al., 2005) driven by Reanalysis meteorology from the European Centre for Medium-range Weather Forecasts (ECMWF) ERA-Interim (Dee et al., 2011; Uppala et al., 2005). The input meteorological data are at 3-hourly time step and interpolated to $1.0° \times 1.0°$ horizontal resolution with 62 vertical layers.

3.1.2 LPDM: FLEXPART_JRA55

The second model setup is also FLEXPART, but driven by the Japanese 55-year Reanalysis (JRA55) from Japanese Meteorological Agency (JMA, Kobayashi et al., 2015; Harada et al., 2016). JRA55 is at 6 hourly time step and on TL319 (~$0.5625°$, ~55 km) horizontal resolution with 60 vertical layers. For this study, we use the JRA55 dataset at the lower resolution (~$1.25°$). This model setup was used for a global inverse modelling system by Global Eulerian-Lagrangian Coupled Atmospheric Model (GELCA) that is a coupled atmospheric model of NIES-TM and FLEXPART (Ishizawa et al., 2016). The primary meteorological observational data for JRA55 have been supplied by ECMWF. In addition to the ECMWF data, the observational data obtained by JMA and other sources are also used.

2.1.3 LPDM:WRF-STILT

The third model setup uses Stochastic, Time-Inverted, Lagrangian Transport Model (STILT) (Lin et al., 2003; Lin and Gerbig, 2005). The wind fields to drive STILT are from the Weather Research and Forecasting model (WRF) (Skamarock et al., 2008) at 10 km resolution. Detailed descriptions are found elsewhere (Hu et al., 2018; Miller et al., 2014; Henderson et al., 2015). The footprints are aggregated to $1.0° \times 1.0°$ horizontal resolution, similar to the other models in this study. The STILT footprint data are provided from CarbonTracker-Lagrange that is a Lagrangian assimilation framework developed at NOAA Earth System Research Laboratory (https://www.esrl.noaa.gov/gmd/ccgg/carbontracker-lagrange/).

3.1.4 Global background model: NIES-TM

The background or initial condition for the LPDMs is obtained by sampling a global model of CH_4 at the 5-day back endpoint locations of the LPDM particles. The global background field of CH_4 mixing ratio is simulated by NIES-TM version 8.1i (Belikov et al., 2013) with the optimised CH_4 fluxes with GELCA-CH_4 inversion system (Ishizawa et al., 2016; Saunois et al., 2016). The GELCA-CH_4 inverse modelling system optimised the monthly CH_4 fluxes for 2000-2015 to assimilate a global network of surface CH_4 measurements available through GAW World Data Center for Greenhouse Gases (WDCGG, http://ds.data.jma.go.jp/gmd/wdcgg). The prior CH_4 fluxes for the GELCA-CH_4 global inversion are also used for the regional inversion in this study as described in the later section. The NIES-TM has $2.5° \times 2.5°$ horizontal resolution and 32 vertical layers, driven by JRA55. For the global simulation, the CH_4 loss in the atmosphere is included; the stratospheric CH_4 loss and OH oxidation schemes are adapted from a model inter-comparison project "TransCom-CH_4" (Patra et al., 2011).

3.2 Prior fluxes

Three cases of prior emissions, labelled as VIS, GEL and WetC, are used as listed in Table 2. Since the global background atmospheric CH_4 field was calculated with GELCA-CH_4 inversion posterior fluxes, we chose the prior (VIS) and posterior (GEL) fluxes from GELCA as two cases of prior fluxes in our regional inversion, respectively. Note that the continuous CH_4 mixing ratio data from the new Canadian Arctic sites were not used in the GELCA-CH_4 inversion. In this study, the mean wetland fluxes for the last 5 years of the GELCA global model were used, and the prior forest fire CH_4 fluxes are detailed in Sect. 3.2.2. The third prior case (WetC) is the same as GEL, but with wetland CH_4 fluxes from WetCHARTs (a recent global wetland methane emission model ensemble for use in atmospheric chemical transport models). WetCHARTs provide inter-annually varying monthly wetland CH_4 fluxes for this study period. The details of prior fluxes are described in the following sections.

3.2.1 Wetland CH$_4$ fluxes

We used the monthly CH_4 wetland fluxes from two different models. The first model is Vegetation Integrative Simulator for Trace gases (VISIT) (Ito and Inatomi, 2012). VISIT is a process-based model, using GLWD as wetland extent. Beside wetland CH_4 flux, VISIT calculates soil CH_4 uptake and CH_4 emission through rice cultivation. The wetland fluxes combined with CH_4 fluxes from rice cultivation were optimised through the GELCA-CH_4 global inversion as a natural CH_4 flux. The second model is WetCHARTs version 1.0 (Bloom et al., 2017a). WetCHARTs derives wetland CH_4 fluxes as a function of a global scaling factor, wetland extent, carbon heterotrophic respiration and temperature dependence (Bloom et al., 2017b). We used the ensemble mean fluxes over 18 model sets which are available for 2001-2015, using 1) three global scaling factors, 2) two wetland extents: GLWD and GLOBCOVER, 3) CARDAMOM (the global CARbon Data MOdel fraMework) as terrestrial carbon analysis, and 4) three temperature dependent CH_4 respiration functions. The WetCHARTs horizontal resolution is $0.5° \times 0.5°$. The modelled CH_4 fluxes are aggregated into $1.0° \times 1.0°$ for this study. Figure 5 shows the spatial distribution of three wetland CH_4 fluxes for the summer months (July-August). Overall, they are similar, while WetCHARTs (WetC) has stronger emissions in Northwest Territories than the two wetland fluxes from VIS and GEL, which are based on VISIT.

3.2.2 Forest fire CH$_4$ fluxes

GFAS (Global Fire Assimilation System) v1.2 (Kaiser et al., 2012) provides biomass burning (BB) emissions by assimilating Fire Radiative Power (FRP) from the MODerate resolution Imaging Spectrometer (MODIS). The FRP observations are firstly corrected for data gaps and then linked to dry matter combustion rates with CH_4 emission factors. GFAS has a daily temporal resolution and $0.1° \times 0.1°$ horizontal resolution. In this study, the daily fire CH_4 emissions are spatially aggregated into $1.0° \times 1.0°$ resolution for the regional inversion, though monthly fluxes were used for the GELCA global inversion.

3.2.3 Anthropogenic Emission

The anthropogenic CH_4 emissions are provided from EDGAR (Emission Database for Global Atmospheric Research) v4.2FT2010 (http://edgar.jrc.ec.europa.eu), except for rice cultivation. EDGARv4.2FT2010 emission which is originally at $0.1°×0.1°$ resolution is aggregated into $1.0°×1.0°$. Since the EDGARv4.2FT2010 data are available until 2010, the same values for 2010 are used for the years beyond 2010. The CH_4 emission from rice cultivation was replaced with the one from VISIT-CH_4 and then treated as a part of natural fluxes. Since there is no rice field in the Canadian Arctic and the rest of North American Arctic/Boreal region, the influence of CH_4 emission from rice cultivation in the region of interest in this study is negligible. The difference of the optimised anthropogenic emissions in the Canadian Arctic from the prior by the global GELCA inversion is almost negligible (from 0.0247 TgCH$_4$ yr^{-1} to 0.0250 TgCH$_4$ yr^{-1}). Compared to the wetland emissions, the anthropogenic emissions are substantially smaller and localised (see Fig. 5).

3.2.4 Other natural CH_4 fluxes

For other natural CH_4 fluxes, we usea map of climatological termite emissions from Fung et al. (1991) and modelled soil uptake from VISIT-CH_4. Because of no termite CH_4 emissions in the Canadian Arctic, termite CH_4 emission has no direct impact, but it is included in global simulation for the background CH_4 mixing ratio. The prior soil CH_4 uptake is provided by VISIT-CH_4 as oxidative consumption by methanotrophic bacteria in unsaturated lands. Soil CH_4 uptake has large uncertainty regionally and also globally. Kirschke et al. (2013) reported that global soil uptake ranges from 9 to 47 TgCH$_4$ yr^{-1}. In the Canadian Arctic, the VISIT-modelled soil uptake is weak (0.094 TgCH$_4$ yr^{-1}) but spread widely (Fig. 5). In some parts of the eastern Canadian Arctic, soil uptakes exceed other CH_4 emissions, resulting in negative fluxes/net sink of atmospheric CH_4.

3.3 Inversion Setup

3.3.1 Regional inversion

In this study, we use the Bayesian Inversion approach (Tarantola, 1987; Rodgers, 2000; Enting, 2002). The Bayesian inversion used here optimises the scaling factors of posterior fluxes by minimising the mismatch between modelled and observed mixing ratios with constraints and given uncertainties using the cost function (J) minimisation method.

$$J(\boldsymbol{\lambda}) = (\boldsymbol{y} - \boldsymbol{K}\boldsymbol{\lambda})^T D_\epsilon^{-1} (\boldsymbol{y} - \boldsymbol{K}\boldsymbol{\lambda}) + (\boldsymbol{\lambda} - \boldsymbol{\lambda}_{prior})^T D_{prior}^{-1} (\boldsymbol{\lambda} - \boldsymbol{\lambda}_{prior}) \tag{1}$$

where $\boldsymbol{y}$ (N×1) is the vector of observations (with the background mixing ratio subtracted, see Section 3.1.4). N is the number of time points multiplied by number of stations (N is reduced if observations are missing). $\boldsymbol{\lambda}$ (R×1) is the vector of the posterior scaling factors to be estimated, R is the number of fluxes to be solved. R is two fluxes per sub-regions × number of sub-regions (i.e., 2 to 6 in this study). $\boldsymbol{\lambda}_{prior}$ is the vector of the prior scaling factors which are all initialised to 1 for all sub-regions, and $\boldsymbol{K}$ (N×R) is the matrix of contributions on the observations (N) from all the fluxes (R) of sub-regions. $\boldsymbol{K}$ is a product of two matrices, $\boldsymbol{M}$ (N × LL) and $\boldsymbol{x}$ (LL×R), $\boldsymbol{M}$ is the modelled transport (or footprints in this study), and $\boldsymbol{x}$ is the spatial distribution of the surface fluxes. LL (=LAT×LON) is the dimension of our domain (1°x1° in latitudes (LAT) by longitudes (LON)). A linear regularisation term has been added which is the

second term on the right-hand side of the equation. D_ϵ and D_{prior} are the error covariance matrices. D_ϵ is the prior model-observation error/uncertainty matrix (N×N) where the diagonal elements are $(\sigma_e)^2$. D_{prior} is the prior scaling factor uncertainty matrix (R×R) where the diagonal elements are $(\sigma_{prior})^2$. We assume that the model-observation mismatch errors are uncorrelated each other and the contributions from the sub-regions are uncorrelated. All the off-diagonal elements in D_ϵ and D_{prior} are assumed to be zero. We assigned σ_e = 0.33 for the model-observation error (Gerbig et al., 2013; Lin et al., 2004, Zhao et al., 2009), and σ_{prior} = 0.30 for the prior uncertainty (Zhao et al., 2009). We examined the inversion's sensitivity to these uncertainties by doubling their values. The posterior fluxes changed by less than 5% for all sub-regions (and the different sub-region masks). The results showed the optimised fluxes are not strongly dependent on these prescribed uncertainties. The estimate for λ is calculated according to the expression below.

$$\lambda = \left(K^T D_\epsilon^{-1} K + D_{prior}^{-1}\right)^{-1}\left(K^T D_\epsilon^{-1} y + D_{prior}^{-1}\lambda_{prior}\right) \quad (2)$$

The posterior error variance-covariance, Σ_{post}, for the estimates of λ is calculated,

$$\Sigma_{post} = \left(K^T D_\epsilon^{-1} K + D_{prior}^{-1}\right)^{-1}. \quad (3)$$

We optimise the CH4 fluxes from biomass burning and separately the remaining fluxes (consisting of wetland emission, soil uptake and anthropogenic emission) on a monthly time resolution.

3.3.2 Domain/Sub-regions

For the Canadian Arctic, which consists of three territories, Northwest Territories (NT), Yukon (YT), and Nunavut (NU), we set up three sub-region masks, Mask A, B and C, as shown in Fig. S4. Outside of the Canadian Arctic is treated as one outer region. Regarding the subdivision of the Arctic region, we examined the sensitivity of the flux estimation to the number of sub-regions. As a starting point, the three territories are treated separately (Mask A). Secondly, YT is combined with NT (Mask B). There is no existing measurement site in Yukon and no significant CH4 emissions in prior fluxes. The inversion results in the next section will show that YT could not be reliably constrained as a separate sub-region (model uncertainties made the estimated fluxes in YT fluctuate from positive to negative). As the third region mask, we solve the fluxes for one region of the entire Canadian Arctic (Mask C). Like YT, NU is a weak source region, compared to NT, and weak observational constraint might lead to unrealistic flux estimates. This exercise on the subdivision gives insights on the constraining power of the existing measurements. Table 3 shows all the inversion experiments in this study. We perform totally 27 experiments with 3 prior emission cases, 3 different transport models and 3 different sub-region masks.

3.3.3 Atmospheric Measurements

This regional inversion study used the continuous measurements at BCK, INU, CBY, and CHL for the four years, 2012−2015 (Fig. 2). First, the afternoon mean values are calculated by averaging the hourly data over 4 hours from 12:00 to 16:00 local time so that the observations we use in this study are more regionally representative assuming mid-day is in well-mixed planetary boundary layer. Second, the modelled background mixing ratios, which were described in Sect. 3.1.4, are subtracted from the afternoon mean observations. The differences in mixing ratio between

observations and background were input into the regional inversion system as local contributions. The observational data examined in Sect. 2 have been already pre-screened for possible contaminations due to mechanical/technical problems during sampling or analysing processes. Except for the pre-screening, we did not apply any additional data screening or filtering.

4 Results and Discussions

4.1 Comparison of footprints

Figure 6 shows the mean footprints (mean emission sensitivities) of all 4 sites by the three different LPDMs. There are common features, but there are also noticeable seasonal differences and differences between the models. The spatial coverage is similar, but the sensitivity to emissions around sites depends on the models. Among the models, STILT shows the strongest sensitivity near the sites, while FLEXPART_JRA55 has the weakest sensitivity. All the footprints near the sites for winter season are stronger than summer season. The footprint differences among the models are also significant. STILT appears to be more localised around the sites. These differences indicate that choosing multiple implementations for the atmospheric transport will allow us to reflect some of the uncertainties introduced to our inversion estimate by transport models.

4.2 Signals in the observations (relative to background)

The regional inversion depends on how well local signals can be detected in the observations. Therefore, we first look at the detectability of local/regional fluxes in the observed atmospheric CH_4 mixing ratios. If the amplitude of local signals is comparable to the background contribution, estimated regional fluxes would be more uncertain because local signals would be difficult to distinguish from the background contributions. In Sect. 2.2.2, we examined the synoptic variability in observed CH_4. Here we apply the same procedures to the modelled background CH_4 for the sites to see if the local synoptic signal is distinguishable from the background CH_4. Figure 7 shows the mean monthly SD of modelled background CH_4 to their fitted curves for the case of FLEXPART_EI (other model setups are analogous), along with those of observed CH_4 (SD_PM in Fig. 4) for the 4 sites to be used as observational constraints (BCK, INU, CBY and CHL). In summer, all the SD_PM values of the observations are much larger (up to three times), than the respective background SDs, indicating strong local influence. While, in winter, both the observation SD_PM and the background SD are comparable. Thus, the observations could provide more constraints on the estimated regional fluxes in summer than in winter.

4.3 Comparison of prior and posterior fluxes with different transport models

The inversion experiments outlined in Table 3 were made to estimate the CH_4 fluxes in the Canadian Arctic using atmospheric observations from the four ECCC sites as mentioned in Sect. 3.3.3. We calculated the posterior flux estimates as the mean of the fluxes estimated in the 9 experiments in Table 3 (for each set of sub-region masks). The variations in the flux results (Standard Deviation) are used to represent the flux uncertainty due to transport errors (3 transport models) and prior flux errors (3 prior emission cases). This flux uncertainty is larger than the posterior flux

covariance uncertainty estimates, Eq. (3). Figure 8 shows the monthly posterior fluxes with sub-region masks A and B. The monthly posterior fluxes with mask C are shown in Fig. S5, along with the aggregated fluxes with masks A and B for the entire Canadian Arctic. As shown in Fig. 8a, the fluxes in NT are dominant, and all the posterior fluxes in NT show clear seasonal cycle and inter-annual variations that are reflected in the total fluxes for the entire Canadian

5   Arctic (Fig. S5). In contrast, no clear seasonal pattern is found for NU and YT (Figs. 8a and 8b). The inversion model has difficulty optimising the weak flux regions. As a result, negative mean fluxes, i.e. CH_4 sinks, could appear, especially in YT (Fig. 8a); the negative biomass burning fluxes are "spurious" since the biomass burning CH_4 source cannot be negative. However, a null-flux would be consistent within error bars.

Next, the differences and similarities in the inversion results from the three transport models are summarised.

10   The differences in the flux estimates by the three different transport models can be seen in Fig. 9. Figure 9 displays the results for YT+NT with Mask B by the three different transport models. FLEXPART_JRA55 tends to estimate higher total fluxes than the other models, resulting in higher emissions by ~0.6 $TgCH_4$ yr^{-1} than the average of ~1.8 $TgCH_4$ yr^{-1}. WRF-STILT tends to yield the lowest estimate among the three models, lower by ~0.5 $TgCH_4$ yr^{-1} than the average. The posterior total fluxes by FLEXPART_EI appear to be moderate. In winter, the FLEXPART-EI fluxes

15   are close to zero, same with WRF-STILT. These results are consistent with their footprints (mean emission sensitivities) in Fig. 6. Higher footprint sensitivities near the sites tend to yield lower posterior fluxes and vice versa.

The inter-model differences in the posterior forest fire fluxes (Biomass Burning, BB) are quite noticeable in 2014 that is the extreme fire year in NT. Due to the sporadic nature of the fire events, the differences in transport (transport errors) are evident in the modelled prior CH_4 mixing ratios (Fig. S6c) and could lead to substantial

20   differences in the posterior fluxes (Fig. 9). The WRF-STILT estimated BB in 2014 appears to be moderate (0.23 $TgCH_4$ yr^{-1}), similar to in 2013 (~0.3 $TgCH_4$ yr^{-1}), while the other two models show the highest BB flux estimates (0.55─0.67 $TgCH_4$ yr^{-1}) in 2014, comparable to the prior flux, GFAS estimates.

In contrast, the inter-annual variability in total posterior fluxes is very similar among all three transport model results (as shown in Figs. 8 and S5). The inter-annual variability in the transport models (an intra-model result) appears

25   to be consistent, yielding similar posterior flux inter-annual variability. Since all three different transport models capture this inter-annual variability, it appears to be a robust feature of the CH_4 source/sink in the Canadian Arctic.

Another robust feature appears to be the similarity in the results for the total Arctic emission with different numbers of sub-regions used in the inversion. The sub-region with strong signals in the prior fluxes (NT) and strong observational constraints (BCK and INU within NT) yielded posterior flux results with small uncertainties, while sub-

30   region with weak signals in the prior fluxes (YT) and weak observational constraint (no observations in YT) yielded large uncertainties in the posterior flux estimates. Weak sub-region like YT could be combined with other sub-region (NT) without strong impact on the inversion results. The temporal variations in the inversion results with different numbers of sub-regions (an intra-model result) seem to be a robust feature also. Given that the strong observational constraints and the strong wetland emissions are both located in the central part of the Canadian Arctic, representing

35   the Canadian Arctic as a single region was able to yield reasonable inversion results.

4.4 Comparison with previous estimates

The estimated fluxes for the entire Canadian Arctic in this study are relatively robust in amplitude and temporal variations even with the different prior fluxes and sub-region masking. The mean estimated total CH_4 annual flux for the Canadian Arctic is 1.8 ± 0.6 $TgCH_4$ yr^{-1}. Compared with two previous inversion estimates, our estimate is slightly lower than the mean total flux of 2.14 $TgCH_4$ yr^{-1} (average from 2009─2013) inferred by FLEXINVERT regional inversion (Thompson et al. 2017), but much higher than the estimate of 0.5 $TgCH_4$ yr^{-1} (average from 2006─2010) from the CarbonTracker-CH_4 global inversion (Bruhwiler et al., 2014) (Fig. 10a).

All the estimated fluxes are seasonally high around July and August (Fig. 10b). The mean summertime maximum of our estimates is quite consistent with the one by Thompson et al. (2017), but our estimated fluxes have narrow high summer emission period and low wintertime emission compared with the estimates by Thompson et al. (2017). These temporal differences in estimated fluxes might reflect the observational constraints used in the respective inversions. Thompson et al. (2017) employed a similar type of regional inversion but for the entire northern high latitudes (north of 50˚N). Except for the flask measurement data at CHL, none of the Canadian Arctic sites used in this study was included in Thompson et al. (2017). The strong regional CH_4 signals at INU and BCK in this study appear to yield flux estimates with narrower high summer emission period and lower wintertime wetland emission compared with the estimates by Thompson et al. (2017).

The flux estimate in this study is partitioned into biomass burning (BB), 0.3 ± 0.1 $TgCH_4$ yr^{-1}, and the remaining flux, 1.5 ± 0.5 $TgCH_4$ yr^{-1}. The remaining flux is mainly natural/wetland CH_4 emissions, given that anthropogenic contribution to the total prior fluxes without BB is ~2 % according to the EDGAR prior fluxes. The estimated wetland flux is comparable to the WetCHARTs (wetland) ensemble mean of 1.35 $TgCH_4$ yr^{-1} (Bloom et al. 2017a; 2017b).

The estimated summertime natural CH_4 fluxes show clear inter-annual variability. The higher emissions are estimated for 2012 and 2014 in this study, which is similar to the results from Carbon Arctic Reservoirs Vulnerability Experiment (CARVE) aircraft measurements over Alaska for 2012 to 2014 (Hartery at al., 2018).

4.5 Relationship of fluxes with climate anomalies

Inter-annual variations of estimated CH_4 fluxes are examined in relation to climate parameters, specifically with surface air temperature and precipitation from NCEP reanalysis (Kalnay et al., 1996). First, monthly mean values at the sub-regions as well as the 4-year mean (2012-2015) for each month are calculated, then the monthly anomalies are computed from the monthly mean values and the 4-year mean of the corresponding month. The temperature and precipitation anomalies are aggregated to the respective regions, NT, YT and NU. On the regional level, climate anomalies in NT and NU are quite similar, though YT is less similar to NT and NU. YT is mainly covered by mountains with little wetland. Furthermore, among the three Arctic territories, NT has the largest wetland extent and most of the forest fire emissions in 2012-2015. Thus, we look into the correlation in monthly anomalies of CH_4 fluxes with summer climate anomalies in NT.

In Fig. 11, the inter-annual variability of wetland CH_4 fluxes exhibits a moderate positive correlation with the surface temperature anomaly (r = 0.55) and only weakly correlated with precipitation anomalies (r = 0.11). This

indicates that the hotter summer weather condition stimulates the wetland CH_4 emission, and precipitation appears to have a less immediate or no direct impact on wetland conditions. In prior cases, VIS and GEL, natural CH_4 fluxes (wetland and other fluxes except biomass burning CH_4 flux) are multi-year mean monthly fluxes. Therefore, these prior fluxes have no year-to-year anomalies and no correlation with the meteorological anomalies. Only in WetC, the

5 prior with wetland CH_4 fluxes from WetCHARTs ensemble mean exhibits inter-annual variations, the correlations with temperature and precipitation anomalies are r = 0.26 and r = 0.90 respectively. The posterior natural fluxes with WetC show slightly higher correlations (r=0.55 with temperature, r=0.16 with precipitation) than the mean correlation values. However, overall there is no clear dependency of posterior correlations on the inherent climate anomaly correlations in the prior fluxes. This result indicates that the inter-annual variations in posterior wetland fluxes in this

10 study are mainly determined by the observations, rather than by prior fluxes.

Inter-annual variations of estimated BB CH_4 fluxes show a negative correlation with precipitation (r = -0.41). Also throughout the fire season (June-September), all estimated BB fluxes negatively correlate with precipitation while the prior BB fluxes appear to have no consistent correlations. The inversion results support that dry condition would enhance the forest fire. The estimated BB fluxes show a weakly negative correlation with surface temperature

15 (r = -0.23) on mid-summer average, but the monthly correlations are fluctuating from r = -0.40 to r = 0.47 over the fire season. Since the period is limited in this study (2012─2015), these statistical relationships are still not clear. Also, the relationship of CH_4 emissions with climate conditions could be complex and non-linear (with extreme fires events in some years). More data and analysis are required to characterise the dependency of CH_4 fluxes on climate in the Arctic.

20 **4.6 Comparison of modelled and observed mixing ratios**

The model-observation statistical comparison is shown with the Taylor diagrams of correlation coefficients and normalised standard deviation (NSD) by three different transport models for the four Arctic sites (Fig. 12) using the inversion results with Mask B and prior flux case WetC. At BCK and INU, the correlation coefficients and NSD for each model are improved by the inversion. At these two sites, the observations contain large synoptic signals from the

25 Canadian Arctic wetland and provide strong constraints to the inversions. At INU, the improvement for STILT is noticeable, especially with NSD. This improvement of STILT is explained further below. At CBY and CHL, no significant changes between the prior and posterior results are seen. This indicates that the regional flux in the Canadian Arctic only weakly influences CBY and CHL.

Further investigation has been conducted for INU. Figure S7a shows the time-series of modelled prior and

30 posterior mixing ratios by the three transport models and the observed mixing ratio. The Taylor diagrams in Fig. S7b show the comparison results of modelled mixing ratios with the observations by seasons, summer months (June─September) and winter months (October─May), as well as for the entire period together. The modelled mixing ratios by STILT with the prior fluxes could be much higher than the mixing ratios by the other two models. That results in the higher prior NSD values, especially in winter season. The inversion was able to improve the results by

35 reducing the fluxes and consequently the posterior NSD.

Another qualitative measure of the goodness of fit of the model to the observations is the reduced chi-square statistics (Drosg, 2009; Hughes and Hase, 2010). In the limit of infinite number of data points and the data are independent and normally distributed, the value of reduced chi-square should be 1. The overall reduced chi-squares for all our experiments are in a narrow range of 1.23−1.27. Given that the observations and modelled mixing ratios are not normally distributed (more frequent high mixing ratio events than low mixing ratio events) and the limited amount of observations, there does not seem to be a strong reason to reject the model results.

4.7 Sensitivity tests

4.7.1 Prior fluxes: wetland CH$_4$ fluxes

Wetland CH$_4$ emissions are the dominant flux in the Canadian Arctic. To examine how the prior fluxes impact on the posterior fluxes, two inversion experiments were conducted with modified WetCHARTs fluxes. One is 50 % reduced emissions in the Canadian Arctic, and another is 50 % increased emissions in the Canadian Arctic. The results are shown as mean posterior natural fluxes in Fig. S8. Despite the change in wetland prior emissions, all the posterior fluxes are similar to the ones in the control case; the changes in the posterior fluxes are less than 5% annually. This indicates that the posterior fluxes are not very sensitive to the amplitude/strength of prior fluxes.

4.7.2 Contributions of background CH$_4$ mixing ratios on the posterior fluxes

We used the same background CH$_4$ mixing ratios for the different transport models, which are calculated using the particle endpoints from FLEXPART_JRA55. The idea of using the same background CH$_4$ fields is to focus on the impact of local/regional transport contribution on regional inversion, separating from the background contribution.

One notable feature in the background CH$_4$ mixing ratios is the relatively large synoptic variability, especially in winter compared to the observed CH$_4$, which might contribute to large uncertainties in flux estimation. To examine how sensitive the inversion results are to these temporal variations in the background CH$_4$ mixing ratios, additional experiments with background CH$_4$ with smoothing windows of 5 days, 10 days and 30 days were made (see Fig. S9a). The examples of the results are shown in Figs. S9b and S9c. The posterior fluxes are not strongly dependent on the different background CH$_4$ mixing ratios. Compared with the unsmoothed background case, slightly small values of NSD are found in the model-observation statistical comparison for summer with 30-day smoothing. It seems there are sufficient observations (signal level) above the background CH$_4$ mixing ratios (noise level) to constrain the inversion results (Fig. 7).

5 Conclusions

The Canadian Arctic region is one of the potential enhanced CH$_4$ source regions related to the ongoing global warming (AMAP, 2015). Earth system models differ in their prediction how the carbon loss there will be split up between CO$_2$

and CH_4 emissions. Even current bottom-up and top-down estimates of CH_4 flux in the region vary widely. This study:

1) analysed the measurements of atmospheric CH_4 mixing ratios from 5 sites established in the Canadian Arctic by ECCC, to characterise the observed variations and examine the detectability of regional fluxes;

5   2) estimated the regional fluxes for 4 years (2012–2015) with the continuous observational data of atmospheric CH_4, and also examined the relationship of the estimated fluxes with the climate anomalies.

The observational data analysis reveals large synoptic summertime signals in the atmospheric CH_4, indicating strong regional fluxes (most likely wetland and biomass burning CH_4 emissions) around Behchoko and Inuvik in Northwest Territory, the western Canadian Arctic. The local signals of atmospheric CH_4 also allow inverse models to

10   optimise biomass burning CH_4 flux (emissions due to forest fire), separately from the natural CH_4 fluxes.

The estimated mean total CH_4 annual flux for the Canadian Arctic is 1.8 ± 0.6 $TgCH_4$ yr^{-1} (wetland flux is 1.5 ± 0.5 $TgCH_4$ yr^{-1}, biomass burning flux 0.3 ± 0.1 $TgCH_4$ yr^{-1}). The mean total flux in this study is comparable to another regional flux inversion result of 2.14 $TgCH_4$ yr^{-1} by Thompson et al. (2017), but much higher than the global inversion result of 0.5 $TgCH_4$ yr^{-1} by CarbonTracker-CH_4 (Bruhwiler et al., 2014). The strong regional CH_4 signals

15   at INU and BCK appear to yield flux estimates in this study with narrower high summer emission period and lower wintertime wetland emission compared with the estimates by Thompson et al. (2017).

Clear inter-annual variability is found in all the estimated summertime natural CH_4 fluxes for the Canadian Arctic, mostly due to Northwest Territories. These summertime flux variations are positively correlated with the surface temperature anomaly (r = 0.55). This result indicates that the hotter summer weather condition stimulates the

20   wetland CH_4 emission.

With longer data records and more analysis in the Arctic, inversion CH_4 flux estimates could yield more details on CH_4 emission strength and seasonal cycle (onset and termination of wetland emissions), and dependence of wetland fluxes on climate conditions. More knowledge on the flux and climate relationship could help evaluate and improve bottom-up wetland CH_4 flux models.

25   Next, we will perform a similar study for the CO_2 measurements from these sites to estimate the Canadian Arctic CO_2 fluxes. Estimation of CO_2 and CH_4 fluxes and monitoring how these fluxes change in the future will improve our understanding on the response of the Arctic carbon cycle to climate change, and also yield long-term trends in CO_2 and CH_4 emissions in the Canadian Arctic.

30   **Data availability**

The data measured at ECCC sites used in this study are available upon request to Doug Worthy (doug.worthy@canada.ca). The Alert data are also periodically updated to WDCGG, http://ds.data.jma.go.jp/gmd/wdcgg. The model-related data are available upon request to corresponding author.

Author Contributions

MI and DC designed the research and prepared the manuscript. MI performed data analysis and inversion experiments. DW led the measurement programs and collected the observational data. MI, DC and EC provided footprints (potential emission sensitivities) information for inversions. All authors contributed to the discussion and interpretation of the
5 results.

Competing Interest

Authors declare that they have no conflict of interest.

Acknowledgments

We acknowledge CarbonTracker (CT) Lagrange program for providing the WRF-STILT footprint data for our
10 inversion study. CT_Lagrange has been supported by NOAA Climate Program Office's Atmospheric Chemistry, Carbon Cycle, & Climate (AC4) Program and the NASA Carbon Monitoring System. We would like to extend our gratitude to the conscientious care taken by the program technicians, Robert Kessler and Larry Giroux, and IT support provided by Senen Racki. Appreciation is also forwarded to the Northwest Territories Power Corporation (NTPC) for making available their building facility to house our equipment and tower to string our sampling lines. NTPC
15 also provided IT communication to permit access to our equipment and transmission of data.

References

AMAP: Assesment 2015: Methane as an Arctic clilmate forcer, Arctic Monitoring ans Assessment Programme (AMAP), Oslo, Norway, 2015.

Belikov, D. A., Maksyutov, S., Sherlock, V., Aoki, S., Deutscher, N. M., Dohe, S., Griffith, D., Kyro, E., Morino, I.,
20 Nakazawa, T., Notholt, J., Rettinger, M., Schneider, M., Sussmann, R., Toon, G. C., Wennberg, P. O., and Wunch, D.: Simulations of column-averaged CO_2 and CH_4 using the NIES TM with a hybrid sigma-isentropic (σ-θ) vertical coordinate, Atmos. Chem. Phys., 13, 1713-1732, 10.5194/acp-13-1713-2013, 2013.

Bergamaschi, P., Houweling, S., Segers, A., Krol, M., Frankenberg, C., Scheepmaker, R. A., Dlugokencky, E., Wofsy, S. C., Kort, E. A., Sweeney, C., Schuck, T., Brenninkmeijer, C., Chen, H., Beck, V., and Gerbig, C.: Atmospheric
25 CH_4 in the first decade of the 21st century: Inverse modeling analysis using SCIAMACHY satellite retrievals and NOAA surface measurements, J. Geophys. Res., 118, 7350-7369, 10.1002/jgrd.50480, 2013.

Bloom, A. A., Bowman, K. W., Lee, M., Turner, A. J., Schreder, R., Worden, J. R., Wedner, R. J., Mcdonald, K. C., and Jacob, D. J.: CMS: Global 0.5-deg Wetland Methane Emissions and Uncertainty (WetCHARTs v1.0), ORNL Distributed Active Archive Center, 2017a.

30 Bloom, A. A., Bowman, K. W., Lee, M., Turner, A. J., Schroeder, R., Worden, J. R., Weidner, R., McDonald, K. C., and Jacob, D. J.: A global wetland methane emissions and uncertainty dataset for atmospheric chemical transport models (WetCHARTs version 1.0), Geosci. Model Dev., 10, 2141-2156, 10.5194/gmd-10-2141-2017, 2017b.

Bousquet, P., Ringeval, B., Pison, I., Dlugokencky, E. J., Brunke, E. G., Carouge, C., Chevallier, F., Fortems-Cheiney, A., Frankenberg, C., Hauglustaine, D. A., Krummel, P. B., Langenfelds, R. L., Ramonet, M., Schmidt, M., Steele, L. P., Szopa, S., Yver, C., Viovy, N., and Ciais, P.: Source attribution of the changes in atmospheric methane for 2006–2008, Atmos. Chem. Phys., 11, 3689-3700, 10.5194/acp-11-3689-2011, 2011.

5   Bruhwiler, L., Dlugokencky, E., Masarie, K., Ishizawa, M., Andrews, A., Miller, J., Sweeney, C., Tans, P., and Worthy, D.: CarbonTracker-CH_4: an assimilation system for estimating emissions of atmospheric methane, Atmos. Chem. Phys., 14, 8269-8293, 10.5194/acp-14-8269-2014, 2014.

Chan, D., Yuen C. W., Higuchi, K., Shashkov, A., Liu, J., Chen, J., Worthy, D.: On the CO_2 exchange between the atmosphere and the biosphere: the role of synoptic and mesoscale processes, Tellus, 56B, 194-212, 2004.

10 Chang, R. Y.-W., Miller, C. E., Dinardo, S. J., Karion, A., Sweeney, C., Daube, B. C., Henderson, J. M., Mountain, M. E., Eluszkiewicz, J., Miller, J. B., Bruhwiler, L. M. P., and Wofsy, S. C.: Methane emissions from Alaska in 2012 from CARVE airborne observations, Proc. Natl. Acad. Sci. U.S.A., 111, 16694-16699, 10.1073/pnas.1412953111, 2014

Ciais, P., Sabine, C., Bala, G., Bopp, L., Brovkin, V., Canadell, J., Chhabra, A., DeFries, R., Galloway, J., Heimann,
15   M., Jones, C., Le Quéré, C., Myneni, R. B., Piao, S., and Thornton, P.: Carbon and Other Biogeochemical Cycles, in: Climate Change 2013: The Physical Science Basis. Contribution of Working Group I to the Fifth Assessment Report of the Intergovernmental Panel on Climate Change, edited by: Stocker, T. F., Qin, D., Plattner, G.-K., Tignor, M., Allen, S. K., Boschung, J., Nauels, A., Xia, Y., Bex, V., and Midgley, P. M., Cambridge University Press, Cambridge, United Kingdom and New York, NY, USA, 465–570, 2013.

20 Cooper, O. R., Parrish, D. D., Stohl, A., Trainer, M., Nédélec, P., Thouret, V., Cammas, J. P., Oltmans, S. J., Johnson, B. J., Tarasick, D., Leblanc, T., McDermid, I. S., Jaffe, D., Gao, R., Stith, J., Ryerson, T., Aikin, K., Campos, T., Weinheimer, A., and Avery, M. A.: Increasing springtime ozone mixing ratios in the free troposphere over western North America, Nature, 463, 344, 10.1038/nature08708

Dee, D. P., Uppala, S. M., Simmons, A. J., Berrisford, P., Poli, P., Kobayashi, S., Andrae, U., Balmaseda, M. A.,
25   Balsamo, G., Bauer, P., Bechtold, P., Beljaars, A. C. M., van de Berg, L., Bidlot, J., Bormann, N., Delsol, C., Dragani, R., Fuentes, M., Geer, A. J., Haimberger, L., Healy, S. B., Hersbach, H., Hólm, E. V., Isaksen, L., Kållberg, P., Köhler, M., Matricardi, M., McNally, A. P., Monge-Sanz, B. M., Morcrette, J. J., Park, B. K., Peubey, C., de Rosnay, P., Tavolato, C., Thépaut, J. N., and Vitart, F.: The ERA-Interim reanalysis: configuration and performance of the data assimilation system, Q. J. R. Meteorolog. Soc., 137, 553-597, 10.1002/qj.828, 2011.

30 Dlugokencky, E. J., Myers, R. C., Lang, P. M., Masarie, K. A., Crotwell, A. M., Thoning, K. W., Hall, B. D., Elkins, J. W. and L. P. Steele, L. P.: Conversion of NOAA atmospheric dry air CH_4 mole fractions to a gravimetrically prepared standard scale, J. Geophys. Res., 110, D18306, doi:10.1029/2005JD006035, 2005.

Drosg, M.: Dealing with Uncertainties: A Guide to Error Analysis Springer-Verlag Berlin Heidelberg, 2009.

Enting, I. G.: Inverse Problems in Atmospheric Constituent Transport, Cambridge University Press, Cambridge, UK,
35   392 pp., 2002.

Fung, I., John, J., Lerner, J., Matthews, E., Prather, M., Steele, L. P., and Fraser, P. J.: Three-dimensional model synthesis of the global methane cycle, J. Geophys. Res., 96, 13033-13065, 10.1029/91JD01247, 1991.

Gasser, T., Peters, G. P., Fuglestvedt, J. S., Collins, W. J., Shindell, D. T., and Ciais, P.: Accounting for the climate–carbon feedback in emission metrics, Earth Syst. Dynam., 8, 235-253, 10.5194/esd-8-235-2017, 2017.

Gerbig, C., Lin, J. C., Wofsy, S. C., Daube, B. C., Andrews, A. E., Stephens, B. B., Bakwin, P. S., and Grainger, C. A.: Toward constraining regional-scale fluxes of CO2 with atmospheric observations over a continent: 2. Analysis of COBRA data using a receptor-oriented framework, J. Geophys. Res., 108, doi:10.1029/2003JD003770, 2003.

Gloor, M., Bakwin, P., Hurst, D., Lock, L., Draxler, R., and Tans, P.: What is the concentration footprint of a tall tower?, J. Geophys. Res., 106, 17831-17840, 10.1029/2001JD900021, 2001.

Harada, Y., Kamahori, H., Kobayashi, C., Endo, H., Kobayashi, S., Ota, Y., Onoda, H., Onogi, K., Miyaoka, K., and Takahashi, K.: The JRA-55 Reanalysis: Representation of Atmospheric Circulation and Climate Variability, J. Meteor. Soc. Japan, 94, 269-302, 10.2151/jmsj.2016-015, 2016.

Hartery, S., Commane, R., Lindaas, J., Sweeney, C., Henderson, J., Mountain, M., Steiner, N., McDonald, K., Dinardo, S. J., Miller, C. E., Wofsy, S. C., and Chang, R. Y.-W.: Estimating regional-scale methane flux and budgets using CARVE aircraft measurements over Alaska, Atmos. Chem. Phys., 18, 185-202, 10.5194/acp-18-185-2018.

Henderson, J. M., Eluszkiewicz, J., Mountain, M. E., Nehrkorn, T., Chang, R. Y. W., Karion, A., Miller, J. B., Sweeney, C., Steiner, N., Wofsy, S. C., and Miller, C. E.: Atmospheric transport simulations in support of the Carbon in Arctic Reservoirs Vulnerability Experiment (CARVE), Atmos. Chem. Phys., 15, 4093-4116, 10.5194/acp-15-4093-2015, 2015.

Hu, L., Andrews, A. E., Thoning, K. W., Sweeney, C., Miller, J. B., Dlugokencky, E., Tans, P. P., Michalak, A., Mountain, M., Nehrkorn, T., Montzka, S. A., Worthy, D., McKain, K., Michel, S.. Vaughn, B., White, J., Fischer, M., Biraud, S., Basu, S., van der Velde I. R.:Water is the dominant control on interannual variability of North American carbon uptake, submitted to Nature, 2018.

Hughes, I. G., and Hase, T.: Measurements and their Uncertainties: A Practical Guide to Modern Error Analysis, Oxford University Press, New York, 2010.

Ishizawa, M., Mabuchi, K., Shirai, T., Inoue, M., Morino, I., Uchino, O., Yoshida, Y., Belikov, D., and Maksyutov, S.: Inter-annual variability of summertime CO_2 exchange in Northern Eurasia inferred from GOSAT XCO_2, Environ. Res. Lett., 11, 105001, doi:10.1088/1748-9326/11/10/105001, 2016.

Ito, A., and Inatomi, M.: Use of a process-based model for assessing the methane budgets of global terrestrial ecosystems and evaluation of uncertainty, Biogeosciences, 9, 759-773, 10.5194/bg-9-759-2012, 2012.

Jammet, M., Crill, P., Dengel, S., and Friborg, T.: Large methane emissions from a subarctic lake during spring thaw: Mechanisms and landscape significance, J. Geophys. Res., 120, 2289-2305, doi:10.1002/2015JG003137, 2015.

Kaiser, J. W., Heil, A., Andreae, M. O., Benedetti, A., Chubarova, N., Jones, L., Morcrette, J. J., Razinger, M., Schultz, M. G., Suttie, M., and van der Werf, G. R.: Biomass burning emissions estimated with a global fire assimilation system based on observed fire radiative power, Biogeosciences, 9, 527-554, 10.5194/bg-9-527-2012, 2012.

Kalnay, E., Kanamitsu, M., Kistler, R., Collins, W., Deaven, D., Gandin, L., Iredell, M., Saha, S., White, G., Woollen, J., Zhu, Y., Leetmaa, A., Reynolds, R., Chelliah, M., Ebisuzaki, W., Higgins, W., Janowiak, J., Mo, K. C., Ropelewski, C., Wang, J., Roy, J., and Dennis, J.: The NCEP/NCAR 40-Year Reanalysis Project, Bull. Am. Meteorol. Soc., 77, 437-471, 1996.

Karion, A., Sweeney, C., Miller, J. B., Andrews, A. E., Commane, R., Dinardo, S., Henderson, J. M., Lindaas, J., Lin, J. C., Luus, K. A., Newberger, T., Tans, P., Wofsy, S. C., Wolter, S., and Miller, C. E.: Investigating Alaskan methane and carbon dioxide fluxes using measurements from the CARVE tower, Atmos. Chem. Phys., 16, 5383–5398, https://doi.org/10.5194/acp-16-5383-2016, 2016.

5   Kirschke, S., Bousquet, P., Ciais, P., Saunois, M., Canadell, J. G., Dlugokencky, E. J., Bergamaschi, P., Bergmann, D., Blake, D. R., Bruhwiler, L., Cameron-Smith, P., Castaldi, S., Chevallier, F., Feng, L., Fraser, A., Heimann, M., Hodson, E. L., Houweling, S., Josse, B., Fraser, P. J., Krummel, P. B., Lamarque, J.-F., Langenfelds, R. L., Le Quéré, C., Naik, V., O'Doherty, S., Palmer, P. I., Pison, I., Plummer, D., Poulter, B., Prinn, R. G., Rigby, M., Ringeval, B., Santini, M., Schmidt, M., Shindell, D. T., Simpson, I. J., Spahni, R., Steele, L. P., Strode, S. A.,

10   Sudo, K., Szopa, S., van der Werf, G. R., Voulgarakis, A., van Weele, M., Weiss, R. F., Williams, J. E., and Zeng, G.: Three decades of global methane sources and sinks, Nat. Geosci., 6, 813-823, 10.1038/ngeo1955, 2013.

Kobayashi, S., Ota, Y., Harada, Y., Ebita, A., Moriya, M., Onoda, H., Onogi, K., Kamahori, H., Kobayashi, C., Endo, H., Miyaoka, K., and Takahashi, K.: The JRA-55 Reanalysis: General Specifications and Basic Characteristics, J. Meteor. Soc. Japan, 93, 5-48, 10.2151/jmsj.2015-001, 2015.

15   Lehner, B., and Döll, P.: Development and validation of a global database of lakes, reservoirs and wetlands, Journal of Hydrology, 296, 1-22, https://doi.org/10.1016/j.jhydrol.2004.03.028, 2004.

Lin, J. C., Gerbig, C., Wofsy, S. C., Andrews, A. E., Daube, B. C., Davis, K. J., and Grainger, C. A.: A near-field tool for simulating the upstream influence of atmospheric observations: The Stochastic Time-Inverted Lagrangian Transport (STILT) model, J. Geophys. Res.-Atmos., 108, Doi 10.1029/2002jd003161, 2003.

20   Lin, J. C., Gerbig, C., Wofsy, S. C., Andrews, A. E., Daube, B. C., Grainger, C. A., Stephens, B. B., Bakwin, P. S., and Hollinger, D. Y.: Measuring fluxes of trace gases at regional scales by Lagrangian observations: Application to the CO_2 Budget and Rectification Airborne (COBRA) study, J. Geophys. Res., 109, doi:10.1029/2004JD004754, 2004.

Lin, J. C., and Gerbig, C.: Accounting for the effect of transport errors on tracer inversions, Geophys. Res. Lett., 32,

25   10.1029/2004GL021127, 2005.

McGuire, A. D., Anderson, L. G., Christensen, T. R., Dallimore, S., Guo, L., Hayes, D. J., Heimann, M., Lorenson, T. D., Macdonald, R. W., and Roulet, N.: Sensitivity of the carbon cycle in the Arctic to climate change, Ecol. Monogr., 79, 523-555, 10.1890/08-2025.1, 2009

Melton, J. R., Wania, R., Hodson, E. L., Poulter, B., Ringeval, B., Spahni, R., Bohn, T., Avis, C. A., Beerling, D. J.,

30   Chen, G., Eliseev, A. V., Denisov, S. N., Hopcroft, P. O., Lettenmaier, D. P., Riley, W. J., Singarayer, J. S., Subin, Z. M., Tian, H., Zürcher, S., Brovkin, V., van Bodegom, P. M., Kleinen, T., Yu, Z. C., and Kaplan, J. O.: Present state of global wetland extent and wetland methane modelling: conclusions from a model inter-comparison project (WETCHIMP), Biogeosciences, 10, 753-788, 10.5194/bg-10-753-2013, 2013.

Michalak, A. M., Bruhwiler, L., and Tans, P.: A geostatistical approach to surface flux estimation of atmospheric trace

35   gases, J. Geophys. Res., 109, 10.1029/2003jd004422, 2004.

Miller, S. M., Miller, C. E., Commane, R., Chang, R. Y.-W., Dinardo, S. J., Henderson, J. M., Karion, A., Lindaas, J., Melton, J. R., Miller, J. B., Sweeney, C., Wofsy, S. C., and Michalak, A. M.: A multiyear estimate of methane

fluxes in Alaska from CARVE atmospheric observations, Global Biogeochem. Cycles, 30, 1441-1453, doi:10.1002/2016GB005419, 2016.

Miller, S. M., Worthy, D. E. J., Michalak, A. M., Wofsy, S. C., Kort, E. A., Havice, T. C., Andrews, A. E., Dlugokencky, E. J., Kaplan, J. O., Levi, P. J., Tian, H., and Zhang, B.: Observational constraints on the distribution, seasonality, and environmental predictors of North American boreal methane emissions, Global Biogeochem. Cycles, 28, 146-160, 10.1002/2013GB004580, 2014.

Nakazawa, T., Ishizawa, M., Higuchi, K., and Trivett, N. B. A.: Two curve fitting methods applied to CO_2 flask data, Environmtrics, 8, 197-218, 1997.

Olefeldt, D., Goswami, S., Grosse, G., Hayes, D., Hugelius, G., Kuhry, P., McGuire, A. D., Romanovsky, V. E., Sannel, A. B. K., Schuur, E. A. G., and Turetsky, M. R.: Circumpolar distribution and carbon storage of thermokarst landscapes, Nature Communications, 7, 13043, 10.1038/ncomms13043, 2016.

Patra, P. K., Houweling, S., Krol, M., Bousquet, P., Belikov, D., Bergmann, D., Bian, H., Cameron-Smith, P., Chipperfield, M. P., Corbin, K., Fortems-Cheiney, A., Fraser, A., Gloor, E., Hess, P., Ito, A., Kawa, S. R., Law, R. M., Loh, Z., Maksyutov, S., Meng, L., Palmer, P. I., Prinn, R. G., Rigby, M., Saito, R., and Wilson, C.: TransCom model simulations of CH_4 and related species: linking transport, surface flux and chemical loss with CH_4 variability in the troposphere and lower stratosphere, Atmos. Chem. Phys., 11, 12813-12837, 10.5194/acp-11-12813-2011, 2011.

Poulter , B., Bousquet, P., Canadell, J., G. , Philippe, C., Philippe, Peregon, A., Marielle, S., Arora, V., K., Beerling, D., J. , Victor, B., Chris, D. J., Fortunat, J., Nicola, G., Akihito, I., Thomas, K., Charles, D. K., Kyle, M., Joe, R. M., Changhui, P., Shushi, P., Catherine, P., Ronny, S., William, J. R., Makoto, S., Renato, S., Hanqin, T., Lyla, T., Nicolas, V., David, W., Andy, W., Xiyan, X., Bowen, Z., Zhen, Z., and Qiuan, Z.: Global wetland contribution to 2000–2012 atmospheric methane growth rate dynamics, Environ. Res. Lett., 12, 094013, 2017.

Rodgers, C. D.: Inverse Methods for Atmospheric Sounding: Theory and Practice, World Scientific, 2000.

Sasakawa, M., Shimoyama, K., Machida, T., Tsuda, N., Suto, H., Arshinov, M., Davydov, D., Fofonov, A., Krasnov, O., Saeki, T., Koyama, Y., and Maksyutov, S.: Continuous measurements of methane from a tower network over Siberia, Tellus B, 62, 403-416, 10.1111/j.1600-0889.2010.00494.x, 2010.

Saunois, M., Bousquet, P., Poulter, B., Peregon, A., Ciais, P., Canadell, J. G., Dlugokencky, E. J., Etiope, G., Bastviken, D., Houweling, S., Janssens-Maenhout, G., Tubiello, F. N., Castaldi, S., Jackson, R. B., Alexe, M., Arora, V. K., Beerling, D. J., Bergamaschi, P., Blake, D. R., Brailsford, G., Brovkin, V., Bruhwiler, L., Crevoisier, C., Crill, P., Covey, K., Curry, C., Frankenberg, C., Gedney, N., Höglund-Isaksson, L., Ishizawa, M., Ito, A., Joos, F., Kim, H. S., Kleinen, T., Krummel, P., Lamarque, J. F., Langenfelds, R., Locatelli, R., Machida, T., Maksyutov, S., McDonald, K. C., Marshall, J., Melton, J. R., Morino, I., Naik, V., O'Doherty, S., Parmentier, F. J. W., Patra, P. K., Peng, C., Peng, S., Peters, G. P., Pison, I., Prigent, C., Prinn, R., Ramonet, M., Riley, W. J., Saito, M., Santini, M., Schroeder, R., Simpson, I. J., Spahni, R., Steele, P., Takizawa, A., Thornton, B. F., Tian, H., Tohjima, Y., Viovy, N., Voulgarakis, A., van Weele, M., van der Werf, G. R., Weiss, R., Wiedinmyer, C., Wilton, D. J., Wiltshire, A., Worthy, D., Wunch, D., Xu, X., Yoshida, Y., Zhang, B., Zhang, Z., and Zhu, Q.: The global methane budget 2000–2012, Earth Syst. Sci. Data, 8, 697-751, 10.5194/essd-8-697-2016, 2016.

Schroeder, R., McDonald, K., Chapman, B., Jensen, K., Podest, E., Tessler, Z., Bohn, T., and Zimmermann, R.: Development and Evaluation of a Multi-Year Fractional Surface Water Data Set Derived from Active/Passive Microwave Remote Sensing Data, Remote Sensing, 7, 15843, 2015.

Schuur, E. A. G., McGuire, A. D., Schadel, C., Grosse, G., Harden, J. W., Hayes, D. J., Hugelius, G., Koven, C. D., Kuhry, P., Lawrence, D. M., Natali, S. M., Olefeldt, D., Romanovsky, V. E., Schaefer, K., Turetsky, M. R., Treat, C. C., and Vonk, J. E.: Climate change and the permafrost carbon feedback, Nature, 520, 171-179, 10.1038/nature14338, 2015.

Skamarock, W. C., Klemp, J. B., Dudhia, J., Gill, D. O., Baker, D. M., Huang, X.-Y., Wang, W., and Powers, J. G.: A Description of the Advanced Reserach WRF Version4, NCAR Technical Notes NCAR/TN-4751STR, 2008.

Stohl, A., Forster, C., Frank, A., Seibert, P., and Wotawa, G.: Technical note: The Lagrangian particle dispersion model FLEXPART version 6.2, Atmos. Chem. Phys., 5, 2461-2474, 10.5194/acp-5-2461-2005, 2005.

Stohl, A., Seibert, P., Arduini, J., Eckhardt, S., Fraser, P., Greally, B. R., Lunder, C., Maione, M., Mühle, J., O'Doherty, S., Prinn, R. G., Reimann, S., Saito, T., Schmidbauer, N., Simmonds, P. G., Vollmer, M. K., Weiss, R. F., and Yokouchi, Y.: An analytical inversion method for determining regional and global emissions of greenhouse gases: Sensitivity studies and application to halocarbons, Atmos. Chem. Phys., 9, 1597-1620, 10.5194/acp-9-1597-2009, 2009.

Tarantola, A.: Inverse Problem Theory: Methods for Data Fitting and Parameter Estimation, Elsevier Sci., New York, 1987.

Tarnocai, C., Canadell, J. G., Schuur, E. A. G., Kuhry, P., Mazhitova, G., and Zimov, S.: Soil organic carbon pools in the northern circumpolar permafrost region, Global Biogeochem. Cycles, 23, doi:10.1029/2008GB003327, 2009.

Thompson, R. L., Sasakawa, M., Machida, T., Aalto, T., Worthy, D., Lavric, J. V., Lund Myhre, C., and Stohl, A.: Methane fluxes in the high northern latitudes for 2005–2013 estimated using a Bayesian atmospheric inversion, Atmos. Chem. Phys., 17, 3553-3572, 10.5194/acp-17-3553-2017, 2017.

Thornton, B. F., Wik, M., and Crill, P. M.: Double-counting challenges the accuracy of high-latitude methane inventories, Geophys. Res. Lett., 43, 12,569-512,577, 10.1002/2016GL071772, 2016.

Uppala, S. M., KÅllberg, P. W., Simmons, A. J., Andrae, U., Bechtold, V. D. C., Fiorino, M., Gibson, J. K., Haseler, J., Hernandez, A., Kelly, G. A., Li, X., Onogi, K., Saarinen, S., Sokka, N., Allan, R. P., Andersson, E., Arpe, K., Balmaseda, M. A., Beljaars, A. C. M., Berg, L. V. D., Bidlot, J., Bormann, N., Caires, S., Chevallier, F., Dethof, A., Dragosavac, M., Fisher, M., Fuentes, M., Hagemann, S., Hólm, E., Hoskins, B. J., Isaksen, L., Janssen, P. A. E. M., Jenne, R., Mcnally, A. P., Mahfouf, J. F., Morcrette, J. J., Rayner, N. A., Saunders, R. W., Simon, P., Sterl, A., Trenberth, K. E., Untch, A., Vasiljevic, D., Viterbo, P., and Woollen, J.: The ERA-40 re-analysis, Q. J. R. Meteorolog. Soc., 131, 2961-3012, doi:10.1256/qj.04.176, 2005.

Worthy, D. E. J., Chan, E., Ishizawa, M., Chan, D., Poss, C., Dlugokencky, E. J., Maksyutov, S., and Levin, I.: Decreasing anthropogenic methane emissions in Europe and Siberia inferred from continuous carbon dioxide and methane observations at Alert, Canada, J. Geophys. Res., 114, 10.1029/2008JD011239, 2009.

Zhao, C., Andrews, A. E., Bianco, L., Eluszkiewicz, J., Hirsch, A., MacDonald, C., Nehrkorn, T., and Fischer, M. L.:
    Atmospheric inverse estimates of methane emissions from Central California, J. Geophys. Res., 114, D16302,
    10.1029/2008JD011671, 2009.

Table 1. ECCC atmospheric measurements sites in the Canadian Arctic.

Site	ID	Latitude [°]	Longitude [°]	Elevation [m]	Sampling height [m]	Start (conti.) Start (flask)
Alert	ALT	82.5N	62.5W	200	10	1988/01 1999/10
Behchoko[a]	BCK	62.8N	115.9W	160	60	2010/10 NA
Inuvik[a]	INU	68.3N	133.5W	113	10	2012/02 2012/05
Cambridge Bay[a]	CBY	69.1N	105.1W	35	10	2012/12 2012/12
Baker Lake	BKL	64.3N	96.0W	95	10	2014/06 2017/07
Churchill[a]	CHL	58.7N	93.8W	29	60	2007/05 2011/10

[a] The sites are used in the inversion in this study

Table 2. Three cases of prior emissions.

Source	VIS	GEL	WetC
Wetland[1]	VISIT	VISIT (optimized, as Natural[1])	WetCHARTs Extended (Ver.1.0)
Soil Uptake[2]	VISIT	VISIT (optimized, as Soil Uptake[2])	VISIT (optimized, as Soil Uptake[2])
Anthropogenic[3] (excl. Rice cultivation)	EDGARv4.2FT2010	EDGARv4.2FT2010 (optimized as Anthropogenic[3])	EDGARv4.2FT2010 (optimized as Anthropogenic[3])
Biomass Bunning[4]	GFASv1.2	GFASv1.2	GFASv1.2
Rice cultivation[1]	VISIT	VISIT (optimized, as Natural[1])	VISIT (optimized, as Natural[1])
Termites[1]	GISS	GISS (optimized, as Natural[1])	GISS (optimized, as Natural[1])

VIS used the same prior fluxes with those for global GELCA-CH_4 inversion except Biomass Burning. GELCA-CH_4 inversion optimised CH_4 fluxes for 4 source types, 1) natural, 2) soil uptake, 3) anthropogenic and 4) biomass burning, which are also indicated by superscripted numbers. GEL used the posterior fluxes from global GELCA-CH_4 inversion. For VIS and GEL, five-year mean of each source type was used. WetC used WetCHARTs extended mean fluxes as wetland CH_4, while other fluxes were same with GEL. For all the scenarios, GFAS v1.2 daily fluxes are used as biomass burning.

Table 3. Experiment configurations. Using each of 3 different masks (A, B and C in Fig. S3), 9 inversion runs were conducted with a combination of 3 prior emission cases (VIS, GEL and WetC on Table 2) and 3 different models (FLEXPART_EI, FLEXPART_JRA55 and WRF-STILT). Totally 27 inversion runs were conducted.

Exp	Mask					
	Mask A (NT, YT, NU)		Mask B (NT+NT, NU)		Mask C (NT+NT+NU)	
	Fluxes	Model	Fluxes	Model	Fluxes	Model
Exp1	VIS	FLEXPART_EI	VIS	FLEXPART_EI	VIS	FLEXPART_EI
Exp2	VIS	FLEXPART_JRA55	VIS	FLEXPART_JRA55	VIS	FLEXPART_JRA55
Exp3	VIS	WRF-STILT	VIS	WRF-STILT	VIS	WRF-STILT
Exp4	GEL	FLEXPART_EI	GEL	FLEXPART_EI	GEL	FLEXPART_EI
Exp5	GEL	FLEXPART_JRA55	GEL	FLEXPART_JRA55	GEL	FLEXPART_JRA55
Exp6	GEL	WRF-STILT	GEL	WRF-STILT	GEL	WRF-STILT
Exp7	WetC	FLEXPART_EI	WetC	FLEXPART_EI	WetC	FLEXPART_EI
Exp8	WetC	FLEXPART_JRA55	WetC	FLEXPART_JRA55	WetC	FLEXPART_JRA55
Exp9	WetC	WRF-STILT	WetC	WRF-STILT	WetC	WRF-STILT
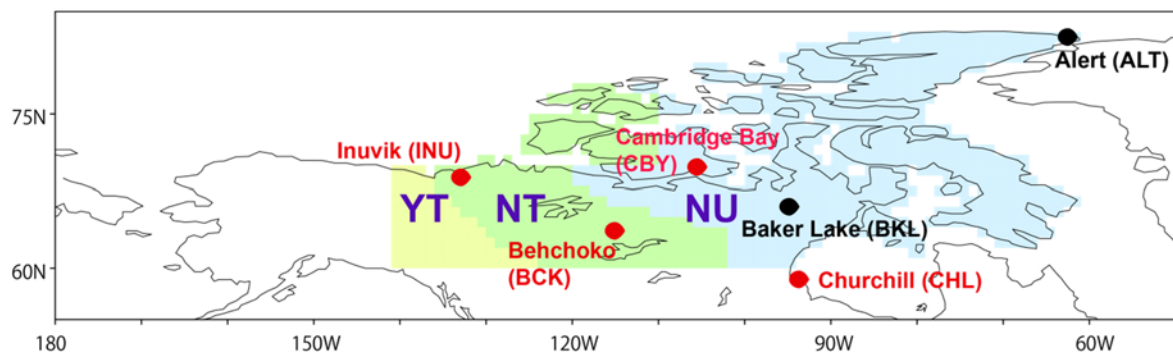
Figure 1: The ECCC atmospheric measurement sites around the Arctic. The sites used for the inversion are indicated in red. The three shaded areas are the three territories which are used as sub-regions in the inversions: YT (Yukon), NT (Northwest Territories) and NU (Nunavut).
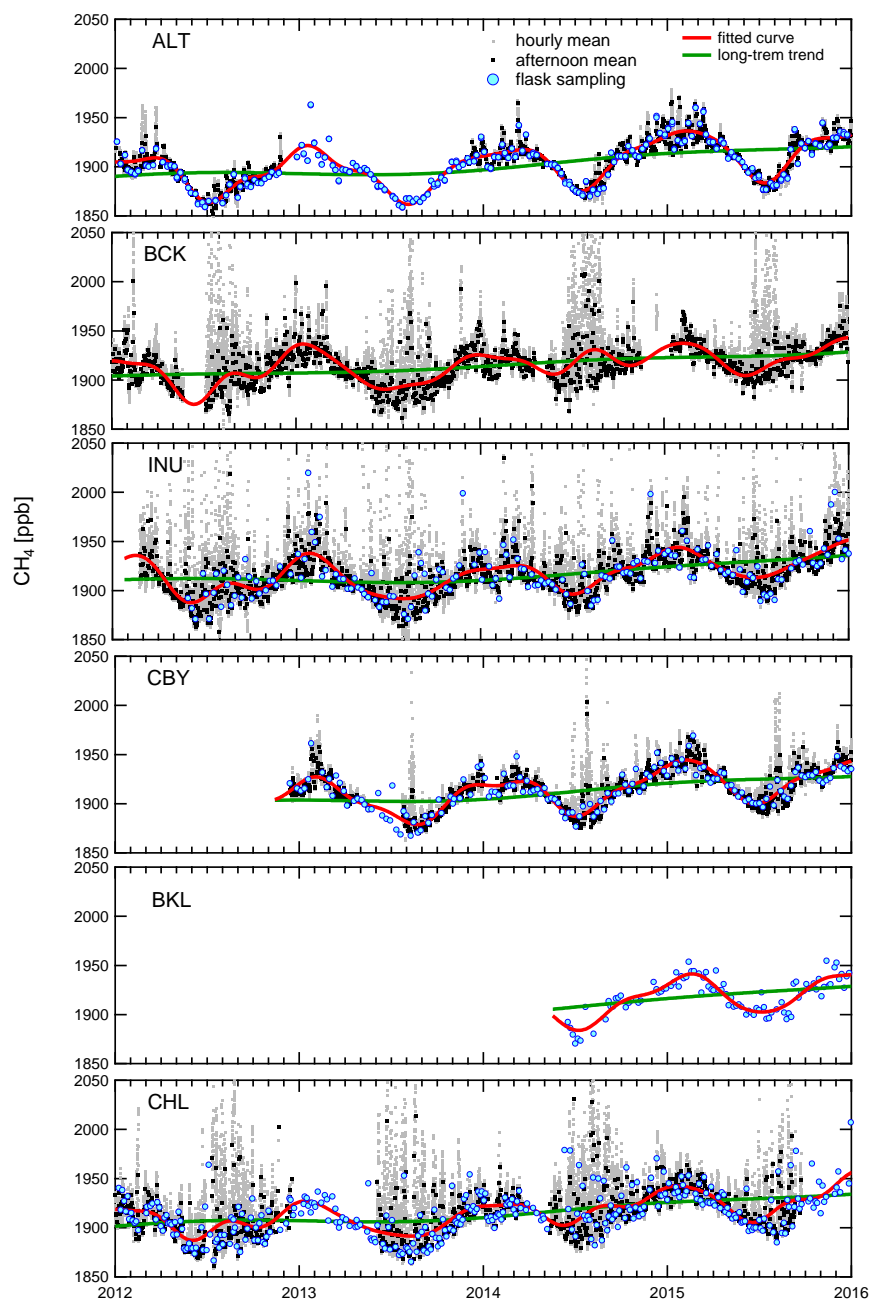
Figure 2: Time-series of atmospheric CH₄ mixing ratios at Canadian Arctic sites. The observed values are the hourly means (grey dot), the afternoon means (black dot, 12:00−16:00 local time) from the continuous measurements and the ones from flask sampling (circle in light blue). BCK has only continuous measurements. At BKL, flask air sampling is only available
5 **after being initiated in 2014. The red and green curves are fitted curves and long-term trends which are obtained by applying a fitting-curve method to the observed afternoon means.**
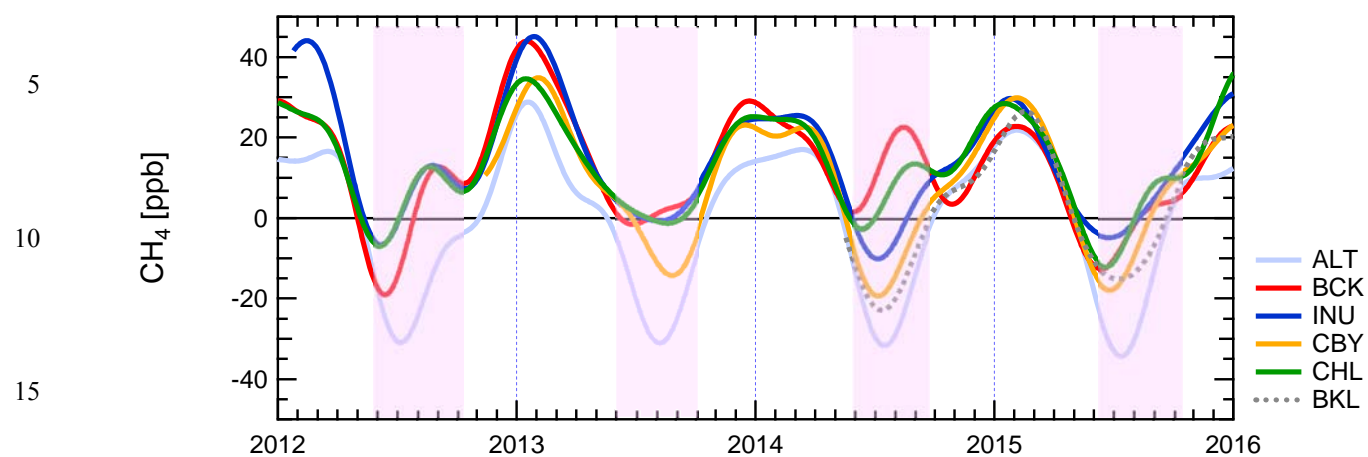
Figure 3: Seasonal components in fitted curves of observed atmospheric CH₄ mixing ratios at Canadian Arctic Sites. Each fitted curve has subtracted the long-term trend component of Alert. Summer months (June–September) are highlighted by light pink shaded background.
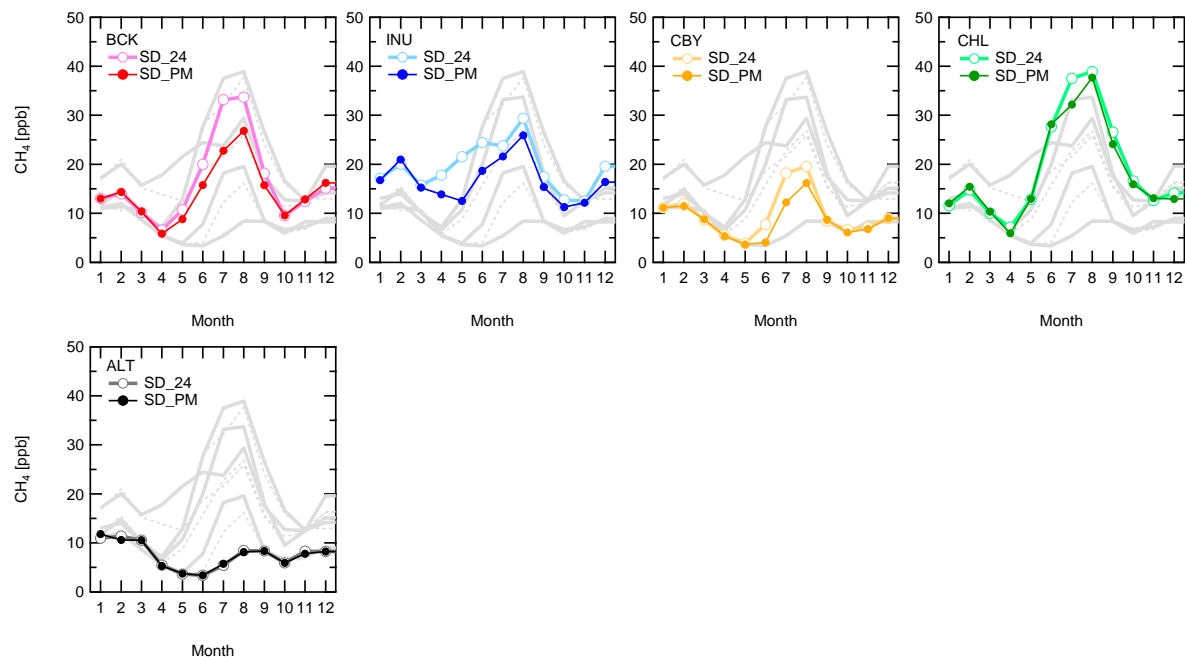
Figure 4: Mean seasonal cycles of monthly standard deviation (SD) of observed CH₄ mixing ratios, SD_24 of all 24 hourly data (closed circles) and SD_PM of afternoon data (12:00−16:00 local time, open circles) to the fitted curves respectively. For BCK, 2014 data have been excluded from the analysis, because of high variability due to massive large forest fires around the site.

VIS | GEL | WetC

Wetland

GELCA Prior (VISIT) | GELCA Posterior | WetCHART Extended

Soil Uptake

GELCA Prior (VISIT) | GELCA Posterior | Same as GEL

Anthropogenic

GELCA Prior (EDGAR) | GELCA Posterior | Same as GEL

Inuvik

Behchoko   Yellowknife

Unit [gCH$_4$/m^2/day]
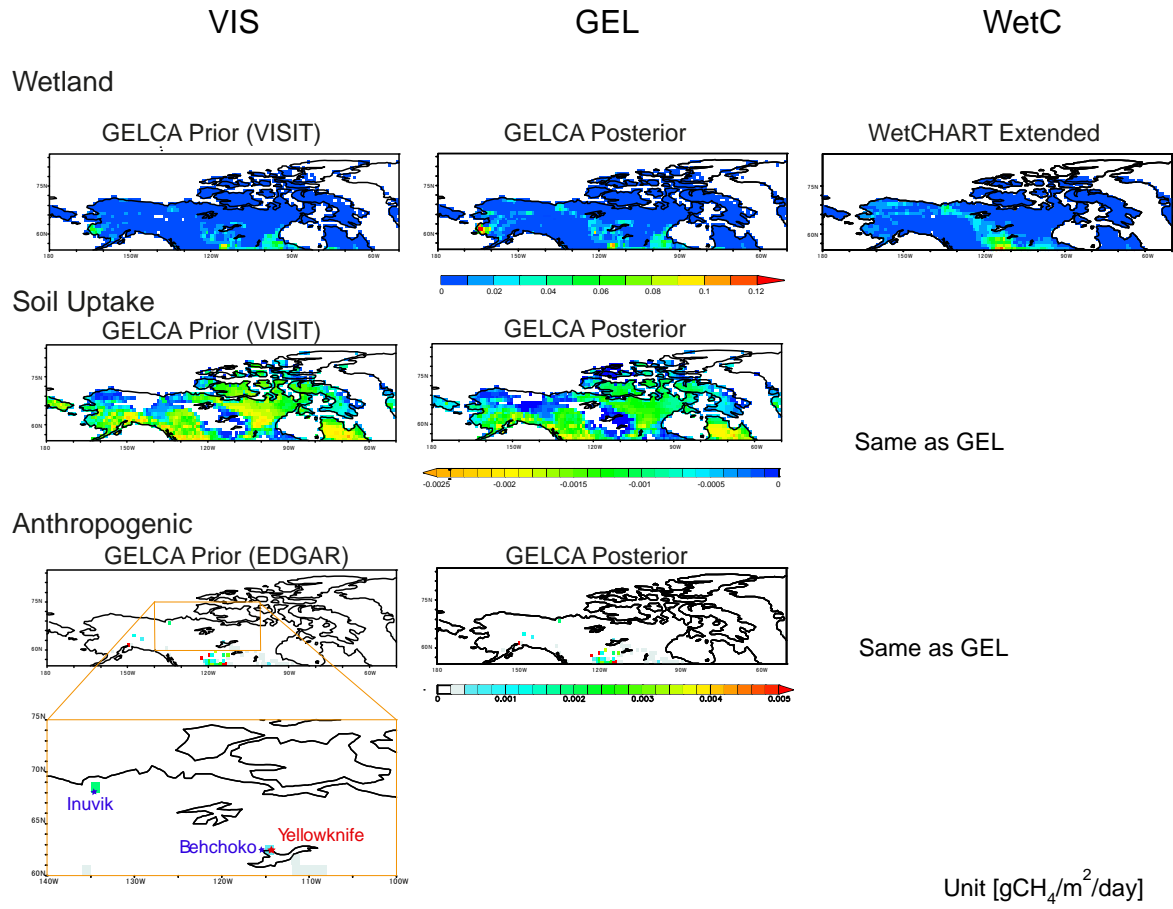
5   **Figure 5: Spatial distributions of summertime prior CH$_4$ fluxes of wetland emission, soil uptake and anthropogenic emissions for the three cases of prior fluxes, VIS, GEL and WetC, which are listed in table 2. Bottom left panel is a zoomed anthropogenic emission distribution in Northwest Territories. The locations of two sites, Behchoko (BCK) and Inuvik (INU) and the capital city, Yellowknife, are also plotted.**
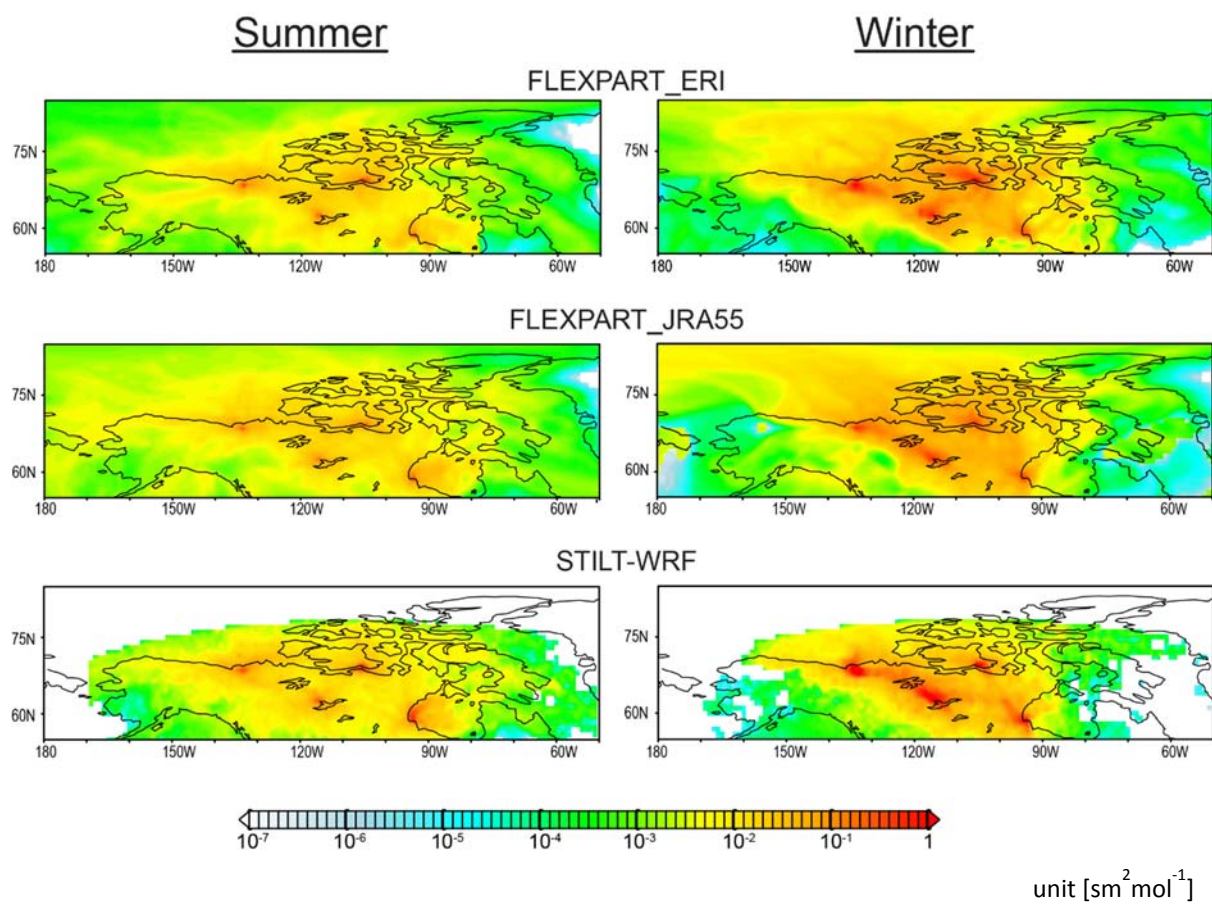
Figure 6: Seasonal mean footprints of all sites by three models, shown for summer, July─August 2013) and winter (January─February 2013).
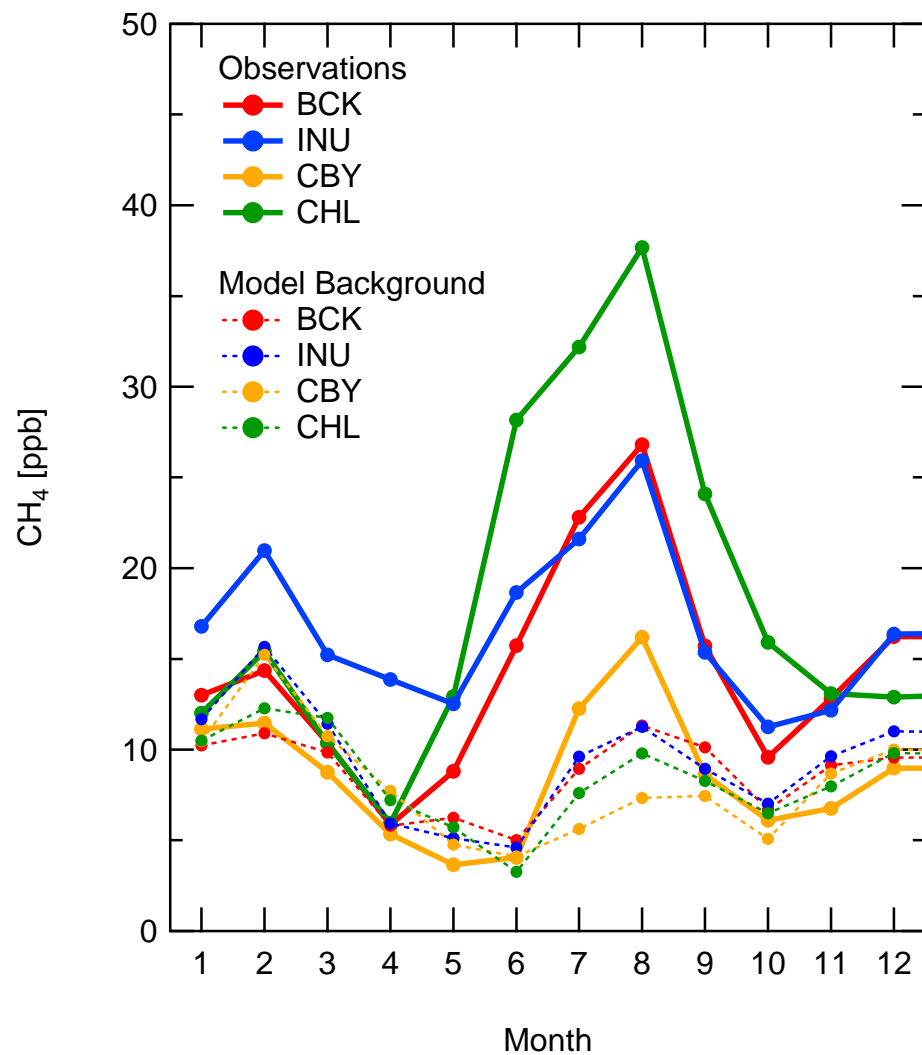
Figure 7: Four-year (2012−2015) mean monthly SD of modelled background CH₄ mixing ratios and SD of observed CH4 mixing ratios (afternoon data only, SD_PM). The background CH₄ mixing ratios are NIES-TM modelled mixing ratios weighted by the endpoints of 5-day back trajectory.
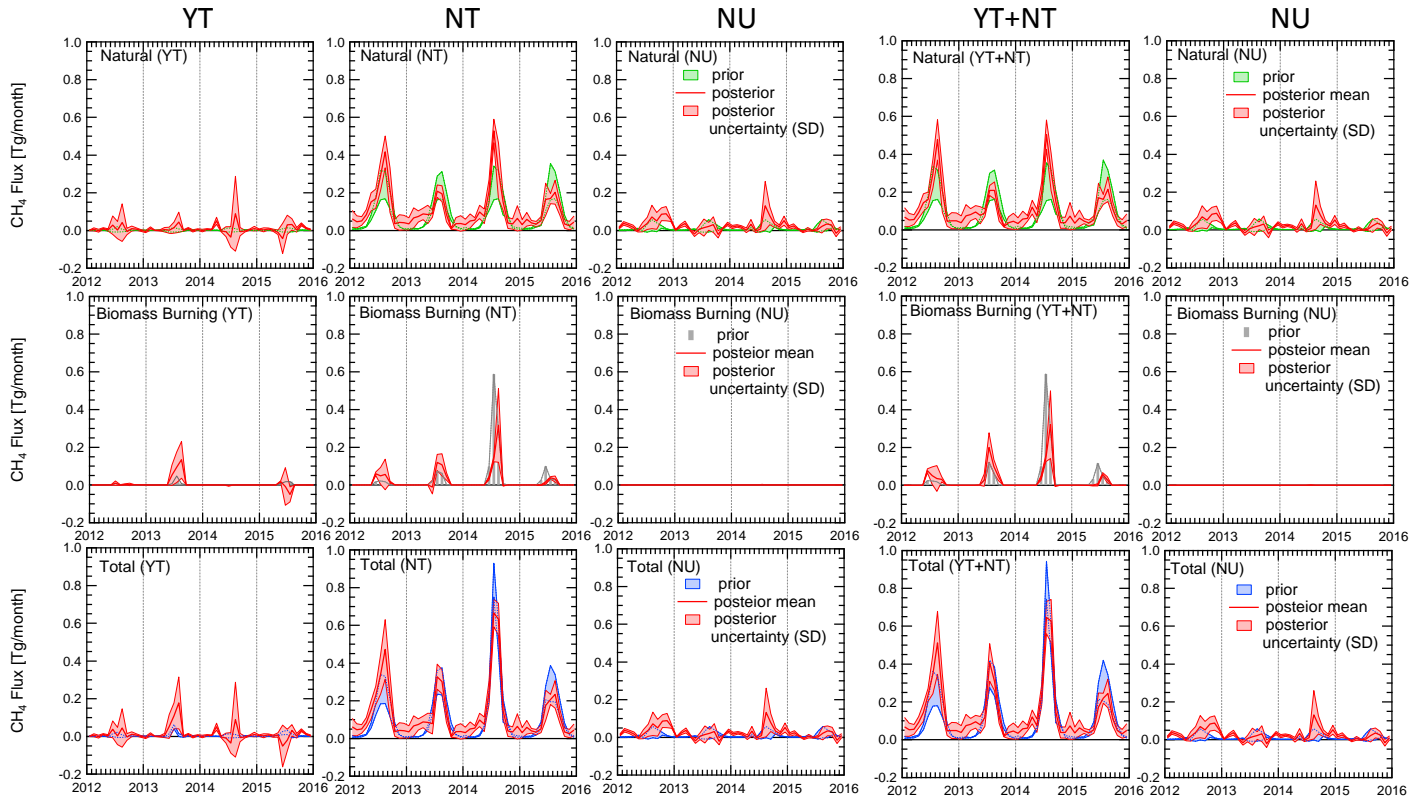
Figure 8: Monthly posterior mean fluxes with (a) sub-region Mask A (YT, NT, NU) and (b) Mask B (YT+NT, NU). Posterior mean flux is an average of nine experiments with 3 models (FLEXPART_EI, FLEXPART_JRA55 and WRF-STILT) and 3 prior emission cases (VIS, GEL and WetC). The posterior SD is shown by the red shaded area. Prior fluxes for natural include wetland flux, soil uptake and anthropogenic emissions. Biomass burning prior fluxes are from GFAS. The (non-red) shaded areas for natural and total prior fluxes indicate the range of prior fluxes.
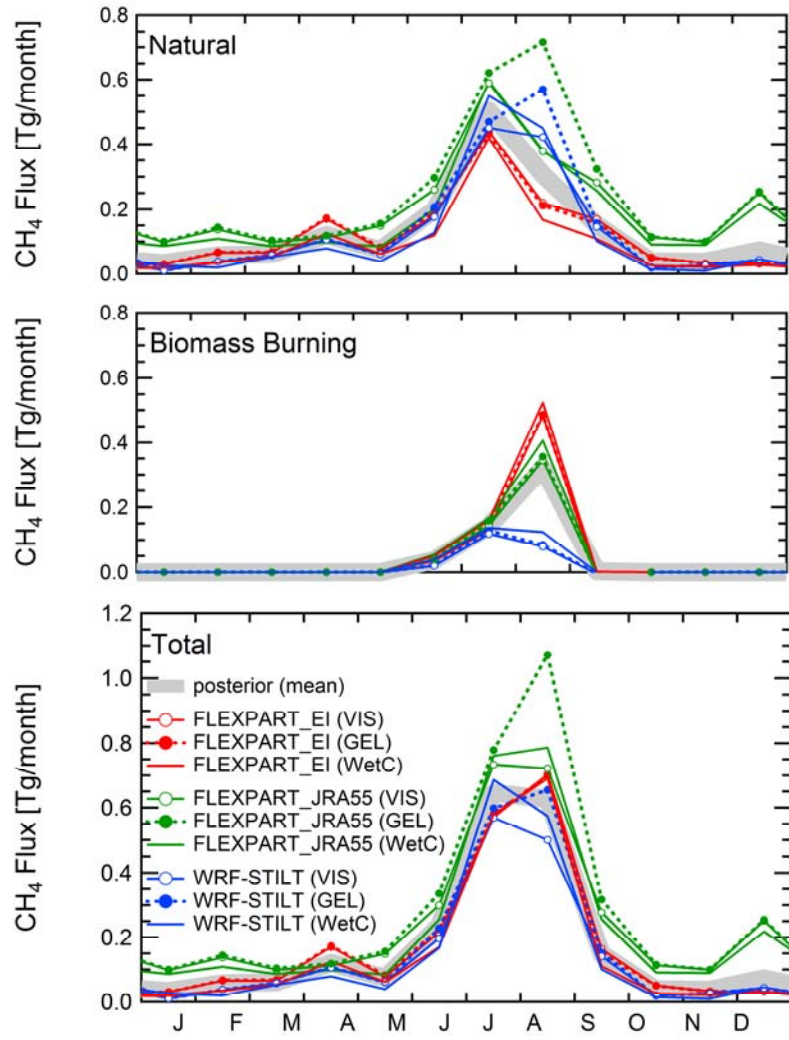
Figure 9: Examples of monthly posterior fluxes by 9 inversion experiments of 3 different models (FLEXPART_EI, FLEXPART_JRA55 and WRF-STILT) with 3 prior emission cases (VIS, GEL and WetC). The posterior fluxes are plotted
5 **for sub-region YT+NT in Mask B. The posterior flux means over all nine experiments with Mask B are also plotted.**

(a) Mean annual Fluxes
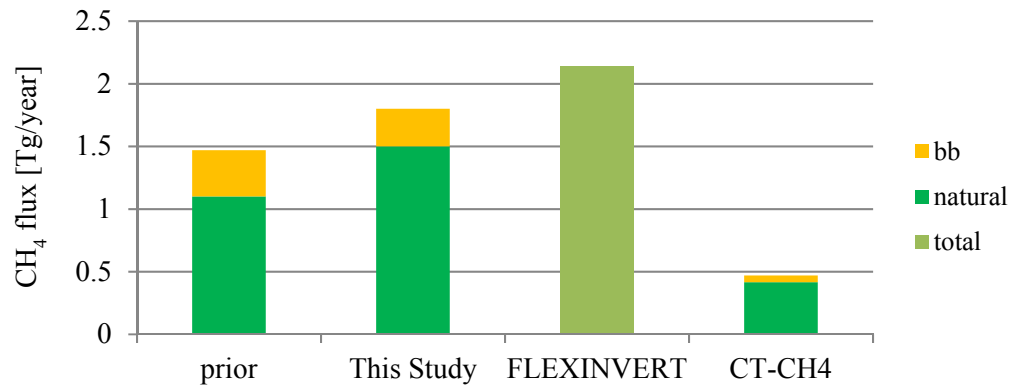
(b) Mean monthly Fluxes
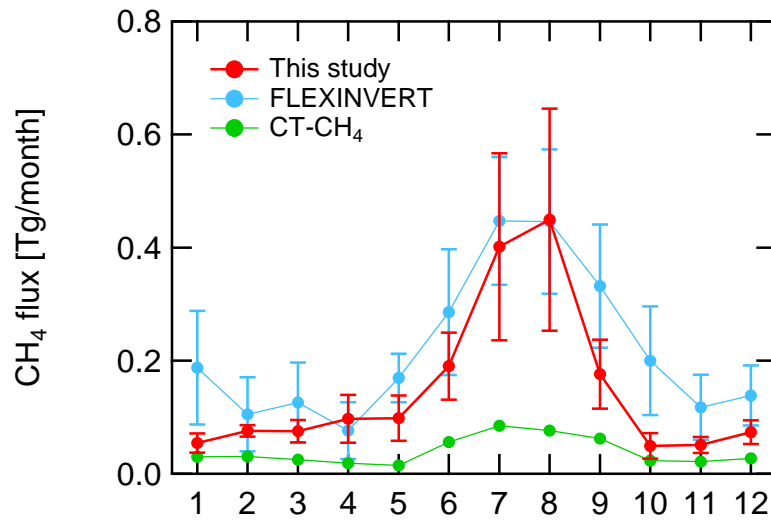
Figure 10: mean prior and posterior (a) annual and (b) monthly fluxes for the Canadian Arctic. FLEXINVERT (Thompson et al., 2017) and CarbonTracker-CH₄ (CT-CH₄, Bruhwiler et al. (2014)) are plotted for comparison. FLEXINVERT and
10 **CT-CH₄ fluxes are their last 5-year means, that is, 2009−2013 and 2006−2010 respectively. "natural" in CT-CH₄ are combined with the fluxes estimated as "anthropogenic" and "agriculture". The bars in monthly fluxes are SD of multi-year mean monthly fluxes.**
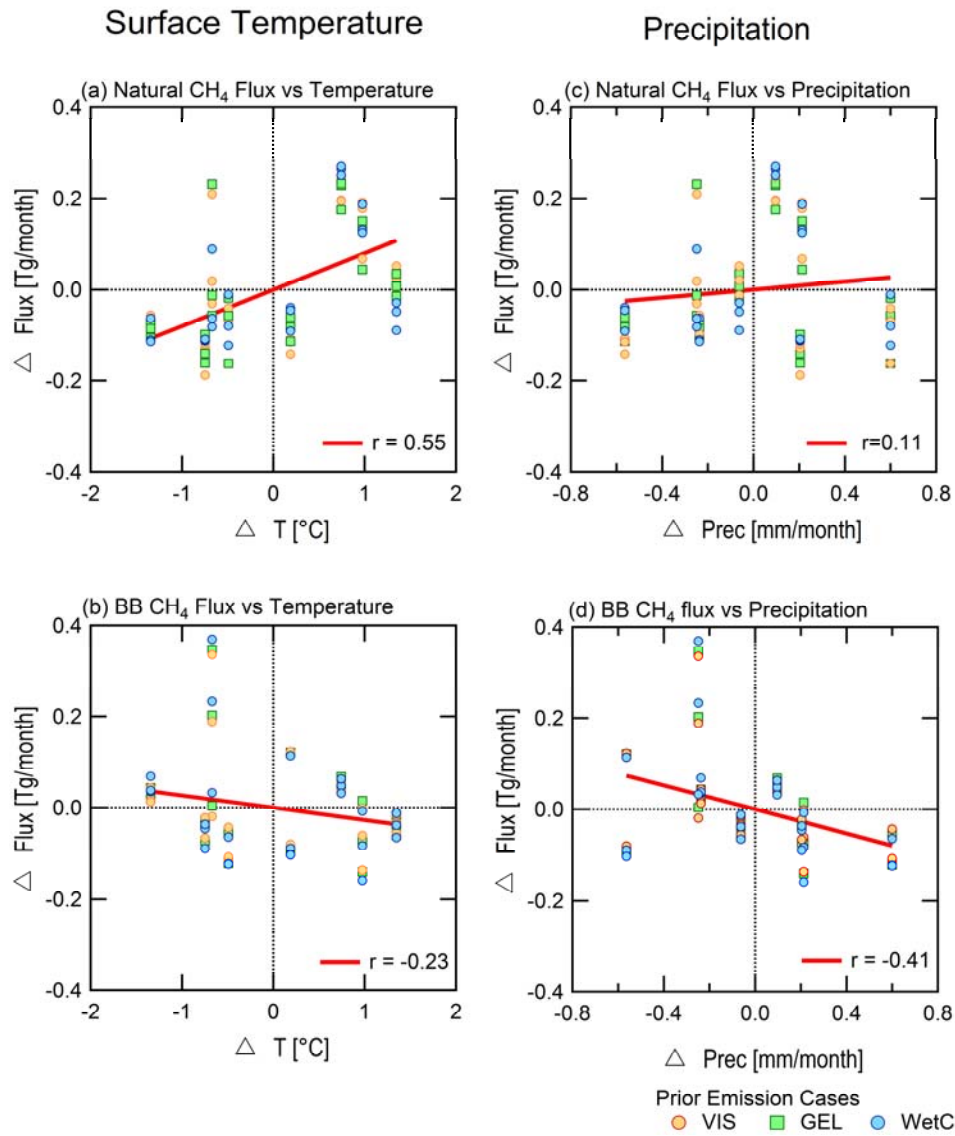
Figure 11: CH₄ flux anomalies vs surface temperature and precipitation anomalies for summer (July and August).   The CH₄ fluxes are July and August posterior fluxes for Northwest Territories (NT) from 9 inversion experiments with Mask A. Regional climate parameter anomalies in NT are monthly deviations from the four-year (2012−2015) means
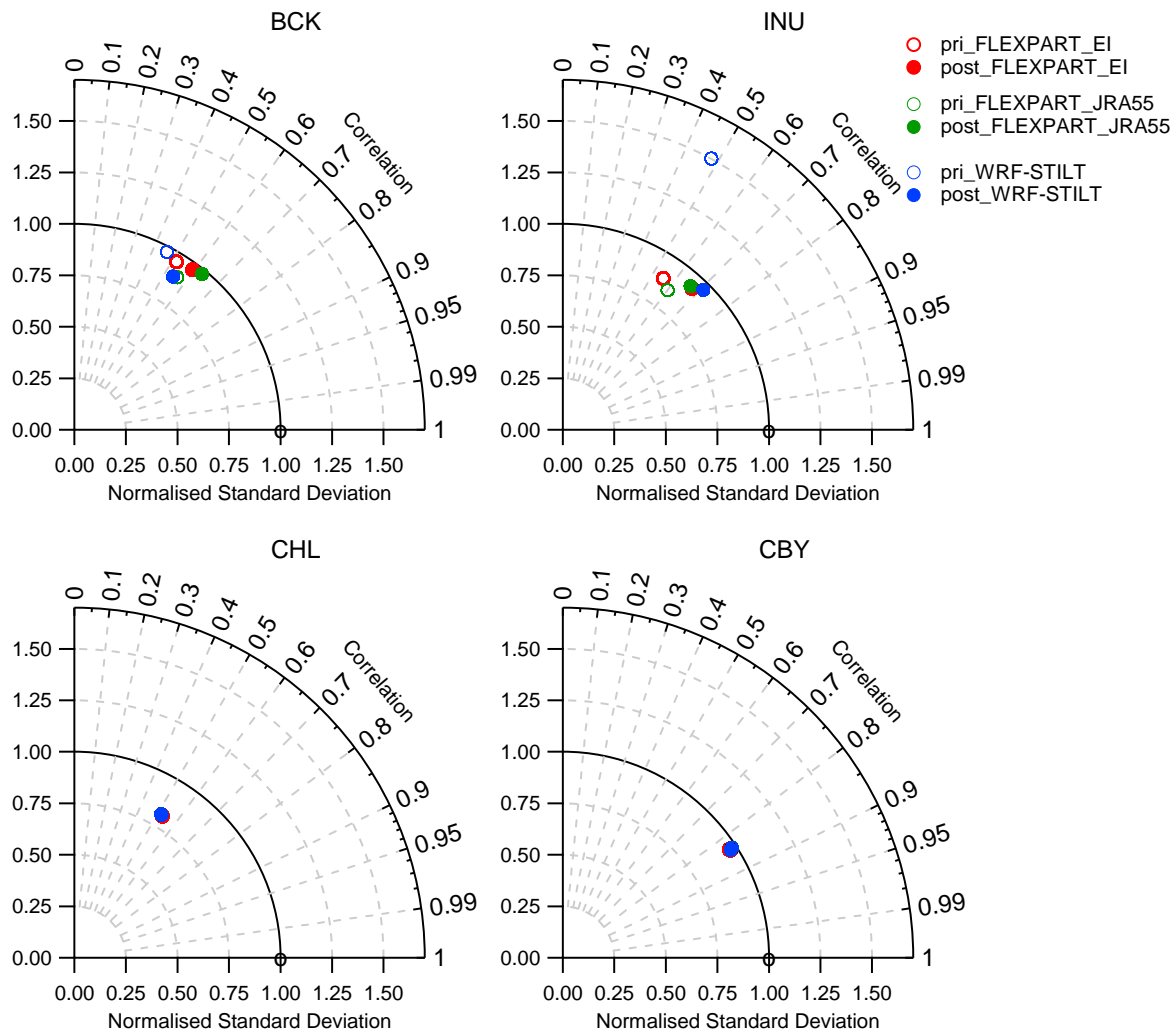
Figure 12: Taylor diagrams for the comparison between the prior (open circles) and posterior (closed circles) mixing ratios by three models: FLEXPART_EI (red), FLEXPART_JRA55 (green), and WRF-STILT (blue), with Mask B and prior flux case WetC. The radius is the normalised standard deviation (NSD) of modelled mixing ratios against observations. The angle is the correlation coefficient. The values are the means with all observations and modelled mixing ratios per each simulation for each site.